Re-analysis of late Quaternary dust mass accumulation rates in Serbia using new luminescence chronology for loess–palaeosol sequence at Surduk

KAJA FENN (iD), JULIE A. DURCAN (iD), DAVID S. G. THOMAS, IAN L. MILLAR AND SLOBODAN B. MARKOVIĆ

BOREAS

Despite numerous palaeoenvironmental investigations of loess–palaeosol sequences across the Carpathian Basin, well-dated high-resolution records are scarce. This paper presents a new high-resolution chronology for the loess-palaeosol sequence at Surduk (Serbia), based on optically stimulated luminescence (quartz) and post-infrared infrared stimulated luminescence (polymineral) dating. The presented record spans 53–19 ka, with primary loess deposition occurring after 52±2 ka, and differs from previously published chronologies that relied on less precise and now superseded dating protocols. Based on the new chronology, mass accumulation rates (MARs) for Surduk were constructed and compared with sites in the Carpathian Basin. The results demonstrate that accumulation periods across this area are not consistent in timing or rates. The high-resolution dating strategy identifies a disturbance in sediment deposition that occurred after 45±2 ka and implies that site contains a hiatus. Finally, we show samples that failed routine dose recovery and preheat plateau tests, and had low fast ratios. Supported by bulk sample geochemical analysis it is proposed that a potential abrupt source shift, during the Last Glacial Maximum, may be the cause of the anomalous luminescence behaviour.

Kaja Fenn (kaja.fenn@ouce.ox.ac.uk), School of Geography and the Environment, University of Oxford, South Parks Rd, Oxford OX1 3QY, UK and Department of Social Sciences, Oxford Brookes University, Headington, Oxford OX3 0BP, UK; Julie A. Durcan and David S. G. Thomas, School of Geography and the Environment, University of Oxford, South Parks Rd, Oxford OX1 3QY, UK; Ian L. Millar, Geochronology and Tracers Facility, British Geological Survey, Keyworth, Nottingham NG12 5GG, UK; Slobodan B. Marković, Faculty of Sciences, University of Novi Sad, Trg Dositeja Obradovića 3, Novi Sad, 21000 Serbia; received 2nd October 2019, accepted 18th March 2020.

Loess–palaeosol deposits in the Carpathian Basin preserve some of the longest, most complete terrestrial records of Quaternary climate change in central Europe (Fitzsimmons *et al.* 2012; Marković *et al.* 2012, 2015). Palaeoenvironmental interpretations of these sedimentary deposits are most valuable when supported by detailed chronologies. Recent advances in radiocarbon dating of loess, utilizing earthworm granules (Moine *et al.* 2017) and mollusc shells (Újvári *et al.* 2014, 2017), are contributing to very high-resolution interpretations of the records. However, the absence of suitable material for radiocarbon dating at some locations, and an upper radiocarbon dating limit of ~50 ka, still present significant limitations to chronology generation. Further, radiocarbon dating provides ages for system closure, i.e. when the exchange of carbon with the environment ceased, which in most cases was when the organism died (Bronk Ramsey 2008), rather than an age for the sediment deposition. Therefore, luminescence dating, which directly dates the burial of sediment grains, is often the most suitable geochronological approach in loess research.

Due to a better understanding of electron transfer within the crystal lattice (e.g. Aitken 1985, 1998; Preusser *et al.* 2008), and athermal stability (Wintle 1973; Murray & Wintle 1999), optically stimulated luminescence (OSL) dating of quartz is usually favoured over the infrared stimulated luminescence (IRSL) of feldspars. However, the use of IRSL signals from feldspars offers an opportunity to date much older material (<500 ka; Thomsen *et al.* 2011), as quartz reaches saturation at 100–200 Gy (Wintle & Murray 2006; Timar-Gabor *et al.* 2015). With the dose rates for quartz varying between ~2.5 and ~4 Gy ka^{-1} in the European loess context (e.g. Schmidt *et al.* 2010; Stevens *et al.* 2011; Fuchs *et al.* 2013; Újvári *et al.* 2014; Perić *et al.* 2019), this provides an upper dating limit approximately of 70 ka when using quartz OSL signals. Attempts to utilize more stable feldspar signals have seen the development of protocols, such as the post-infrared IRSL (pIRIR) protocol (Thomsen *et al.* 2008; Buylaert *et al.* 2011), which accesses more stable signals in comparison to lower temperature IRSL signals, and often bypasses the need for a fading correction (Huntley & Lamothe 2001; Kars *et al.* 2008; Li & Li 2008; Morthekai *et al.* 2008).

Feldspar and polymineral based luminescence chronologies have been generated for numerous sites across the Carpathian Basin including in Serbia, Hungary and Croatia. However, in many locations, such as Albertirsa (Novothny *et al.* 2002), Erdut (Galović *et al.* 2009), Surduk (Fuchs *et al.* 2008), Paks (Frechen *et al.* 1997) and Süttő (Novothny *et al.* 2009), the chronology was determined from IRSL signals that had not been corrected for fading. A recent study used non-fading pIRIR signals rather than IR$_{50}$ signals to re-evaluate the chronology at Paks (Thiel *et al.* 2014). The authors showed that IR$_{50}$ signals fade by approximately 3‰/

decade, suggesting the need for many previously investigated sites to be revisited.

High-resolution, absolute ages provide a basis for mass accumulation rate (MAR) estimations (Kohfeld & Harrison 2003). MARs can provide an additional proxy for the past environmental change at a site (Újvári *et al.* 2017), as they 'normalize' the magnitude and rate of the changes. This not only allows the opportunity to investigate and correlate changes between different loess sites, but also other dust record archives (Frechen *et al.* 2003; Újvári *et al.* 2010; Pigati *et al.* 2013; Perić *et al.* 2019). These data sets also feed into global palaeo-dust cycle models, providing information on the global and regional dust fluxes, and interactions between the atmosphere and dust (Mahowald *et al.* 2006; Muhs 2013; Albani *et al.* 2015).

We present a new luminescence chronology for the loess–palaeosol profile at Surduk, Serbia. A published chronology from a profile ~2 km from our site (Fuchs *et al.* 2008) relied on 10 OSL ages determined using an uncorrected IR_{50} signal obtained using an older, multi aliquot additive-dose measurement protocol (MAAD). Subsequently, research by Antoine *et al.* (2009) supplemented the original chronology with radiocarbon ages and showed that the luminescence chronology was likely underestimating the burial age due to the use of the uncorrected IRSL signal. Here, we present a new chronology based on 13 quartz OSL and 10 polymineral $pIRIR_{220}$ ages. Based on this new chronology, MARs are calculated and discussed in the context of regional and global dust records.

Regional setting and site description

Surduk is part of a long stretch of thick loess deposits along the western bank of the Danube in Serbia, with a number of other sites such as Batajnica (Marković *et al.* 2009) and Stari Slankamen (Marković *et al.* 2011) previously investigated. The site (latitude 45°4′50.24″N, longitude 20°18′50.12″E, altitude 107 m a.s.l.) is situated 2 km northwest from a previously studied profile at Surduk, which was investigated for particle size, magnetic susceptibility, total organic carbon, carbonate content, and carbon isotopes (Fuchs *et al.* 2008; Antoine *et al.* 2009; Hatté *et al.* 2013). Due to access constraints the original site, referred to here as Surduk 1, could not be investigated. The new location analysed here is referred to as Surduk 2.

Surduk 2 is located 7 km downstream of the Danube's confluence with the Tisza River and ~20 km from the Titel Loess Plateau (Fig. 1). The selected loess–palaeosol exposure is located in a gully along a road cutting 200 m from the main river channel. Figure 2 shows a simplified sedimentary succession and sample positions in the investigated Surduk 2 profile. The profile was sampled as two sub-profiles, A and B (Fig. 2), 10 m apart. While fieldwork aimed to ensure the two profiles overlapped, we subsequently suspect that there is a gap of up to 1.5 m between the profiles.

Luminescence dating

Sampling, preparation and measurement

Surduk 2 was sampled for luminescence dating using opaque light tight plastic tubes, hammered into the cleaned loess–palaeosol profile. Seventeen samples were collected at a 30-cm resolution throughout the profile, access permitting. All samples were prepared and analysed at the Oxford Luminescence Dating Laboratory, University of Oxford, under subdued orange-light conditions. To avoid light contamination, sediment from both ends of the sampling tubes was removed and used for particle size and dose rate analysis. All sediment was treated with 32% HCl (~2 h) and 30% H_2O_2 (up to 2 weeks), to remove carbonates and organic matter, respectively. Sieving and settling was used to isolate 4–11 μm grain sizes, which were divided into two fractions: polymineral and quartz. To prepare the quartz enriched fine-grained fraction, samples were additionally treated with H_2SiF_6 (up to 2 weeks) to remove non-quartz minerals, followed by a brief 32% HCl (~2 h) immersion to dissolve any potential fluorite precipitates. In both polymineral and quartz cases, sediment was dispensed onto the surface of 9.7 mm aluminium discs.

Luminescence measurements were made using Risø TL/OSL readers fitted with a calibrated $^{90}Sr/^{90}Y$ beta source and a bialkali photomultiplier tube. For all quartz analyses, OSL signals were measured in a UV detection window through 7.5 mm U-340 glass filters (Bøtter-Jensen *et al.* 2000) by stimulating with blue-light emitting diodes (470 nm). In the case of polymineral aliquots, IRSL signals were detected in the blue-violet region of the electromagnetic spectrum through a combination of Schott BG39/Corning 7-59 filters by stimulation with infra-red light emitting diodes (870 nm).

Dosimetry

Light-exposed sediment from the sampling tubes was dried, homogenized and used to determine radionuclide concentrations for all samples. Concentrations of uranium, thorium, potassium and rubidium were determined by inductively coupled plasma mass spectrometry (ICP-MS) at the British Geological Survey, Keyworth, and converted to infinite-matrix dose rates using the conversion factors of Guérin *et al.* (2011). These dose rates were adjusted for alpha efficiency using a-values of 0.04±0.04 for quartz and 0.11±0.02 for polymineral fractions (Kreutzer *et al.* 2014), grain size attenuation for alpha dose rates by Brennan *et al.* (1991) and Mejdahl (1979) for beta dose rates, and a typical loess moisture content of 15±5% (e.g. Stevens *et al.* 2011; Schatz *et al.* 2012; Újvári *et al.* 2014). Geographical
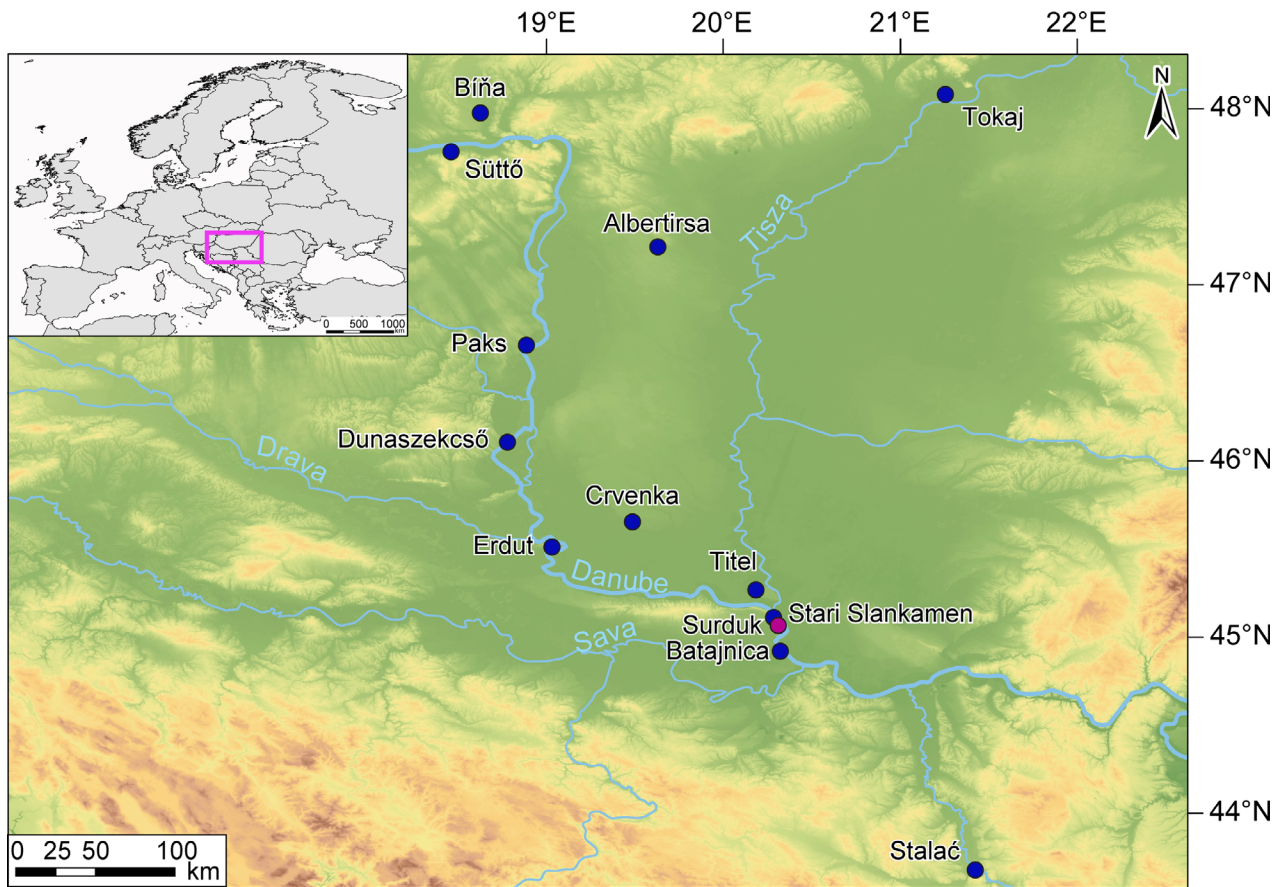
Fig. 1. Map of the study region, study site (Surduk) and other sites discussed in the text (DEM source: ©JAXA, River shapefile: Natural Earth).

location, sediment thickness, and altitude were used to calculate the cosmic dose rate (Prescott & Hutton 1994). All dose rates were calculated using the DRAC (v1.2) software (Durcan *et al.* 2015).

OSL measurements

All of the tests and equivalent doses (D_es) for quartz aliquots were determined using the single aliquot regenerative dose (SAR) protocol (Murray & Wintle 2000; Wintle & Murray 2006). In all cases, luminescence was measured at 125 °C for 40 s following a preheat, while a 160 °C cut-heat was applied for the test dose. D_es were determined by integrating the first 0.5 s of stimulation and by subtracting the background calculated from the last 20 s of stimulation. Depending on the fit, an exponential or an exponential plus linear function was used to fit the dose-response curves.

Preheat plateau

To determine the most appropriate temperature conditions for the quartz SAR protocol, a preheat plateau test

for samples SER16/2/1, SER16/2/7 and SER16/2/9 was conducted. Aliquots were bleached twice for 1000 s with blue light stimulation at 50 °C with a 10 000 s pause in between, before administering a dose approximating a natural one: ~65, ~149 and ~119 Gy, respectively. Three aliquots for each of the six tested temperatures were measured using the SAR protocol described above. Figure 3 shows the results of the quartz preheat plateau. Samples SER16/2/1 and SER16/2/9 show a similar pattern with a drop in the ability to recover the given dose at intermediate temperatures. While a number of temperatures appear suitable, further dose recovery tests at 200 and at 260 °C showed that the latter recovers the dose more accurately. On that basis, a 260 °C preheat temperature was selected for all further tests and D_e determination. In contrast, sample SER16/2/7 performed poorly across the preheat temperature range (Fig. 3) and did not recover the administered dose. Additionally, initial D_e tests showed that all measured discs failed the recycling ratio, suggesting D_e determination using the SAR protocol is not appropriate for this sample. Therefore, no further measurements using the quartz OSL signal were made for this sample.
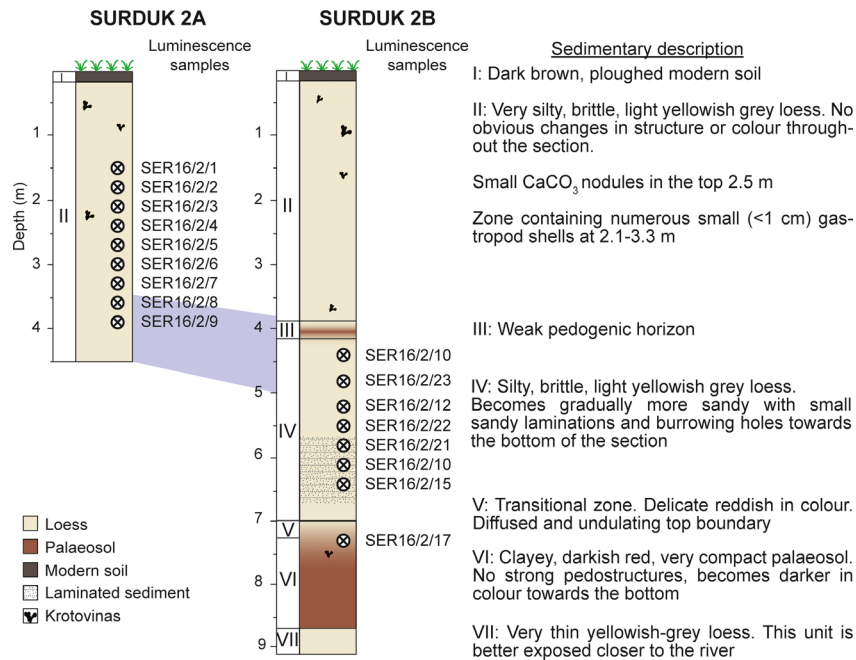
Fig. 2. Stratigraphical logs for Surduk A and B, and sedimentary description for the profile. The blue shading indicates the expected age overlap on the basis of visual correlation in the field.

Dose recovery

To examine the suitability of the selected preheat temperature, and therefore the SAR protocol's ability to recover a laboratory administered dose, dose recovery tests were performed. Three samples (12 aliquots from each) that capture the age spread of the profile were selected. As in the case of the preheat plateau, aliquots were bleached twice and dosed with levels approximating those naturally occurring: ~65 Gy (SER16/2/1), ~69 Gy (SER16/2/3) and ~92 Gy (SER16/2/9). Almost all discs recovered the administered dose within uncertainty (Fig. 4), with an average measured to given dose ratio of 0.94 ± 0.06 ($n = 36$, Table 1), demonstrating the suitability of the quartz SAR protocol to recover a laboratory administered dose.

Quartz signal assessment and provenance

The quartz OSL signal comprises a number of discrete components, fast, medium and slow (e.g. Smith & Rhodes 1994; Bailey *et al.* 1997). Signal from the fast component is preferred for dating because it bleaches rapidly in nature and is thermally stable (Wintle & Murray 2006). To quantitatively test for the dominance of the fast component in the initial part of the OSL signals, the fast ratio (Durcan & Duller 2011) was calculated with the R calc_FastRatio script (King *et al.* 2019). In addition, continuous-wave OSL signals were fitted with the sum of exponentials using the fit_CW-Curve script (Kreutzer 2019) to assess any variability in

the number of components identified, and the relative contribution of signal from the various components to the total OSL signal.

The majority of measured quartz signals decayed rapidly to background levels within a few seconds (Fig. 5A), and qualitatively, this suggests dominance of the fast component. This qualitative assessment is confirmed by the fast ratio, calculated for both natural and regenerated signals, of selected representative samples from Surduk 2A and Surduk 2B (SER16/2/1, SER16/2/3, SER16/2/4, SER16/2/7, SER16/2/8, SER16/2/9, SER16/2/23 and SER16/2/20). Averages above 20 were calculated for all samples, except for the sample SER16/2/8. However, there was a lot of variability between individual discs especially in the samples from Surduk 2B, e.g. for SER16/2/23 fast values range between 8.3 ± 2.9 and 357.9 ± 530.5.

Sample SER16/2/8 had a notably less bright OSL signals and decayed more slowly than other samples (Fig. 5D), with 13 out of 15 signals displaying a fast ratio below 20 (FR average = 13.1 ± 2.3). This suggests that signal from the fast component does not dominate the initial part of the OSL signal, which may result in erroneous D_e determination (Durcan & Duller 2011). On this basis, quartz D_es for this sample are considered unreliable.

The application of routinely applied tests such as preheat plateau, dose recovery, and the fast ratio provides grounds for signal rejection, but does not provide insights into the cause of the signal problems. One avenue to explore is sediment geochemical compo-
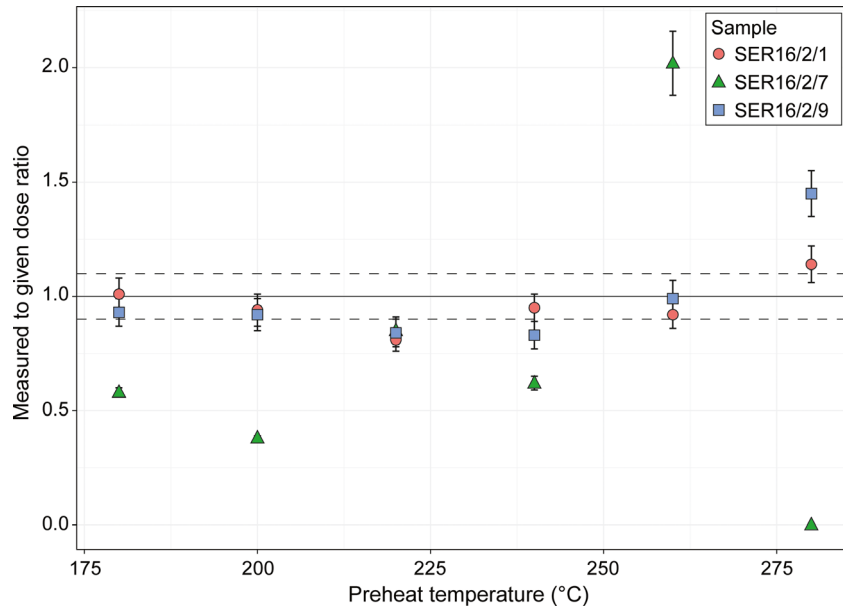
Fig. 3. Preheat plateau for quartz samples SER16/2/1, SER16/2/7 and SER16/2/9. Each point represents an average of three aliquots at each temperature. Dotted lines mark ±10% from unity.

sition to investigate any potential causes of this abrupt shift in quartz behaviour. While much work has been undertaken to establish links between provenance and luminescence dating (cf. Gray *et al.* 2019), only a few studies have looked at geochemical properties for comparison (Götte & Ramseyer 2012; Stevens *et al.* 2013; Rodrigues *et al.* 2019).

Bulk sample geochemical data from ICP analyses were examined in more detail. Trace elements, normalized relative to the upper continental crust (UCC), are shown in Fig. 6A. Negative anomalies relative to the UCC can be seen for Rb, Ba and Sr for all the Surduk 2 samples, which is likely related to the removal of these elements as part of the weathering process and/or low concentrations of feldspars in the samples. The relatively high enrichment of transitional elements (V, Cr and Ni; Fig. 6A) suggests a mafic character of the source rocks (Gasparon *et al.* 1993; Bracciali *et al.* 2007), especially in samples SER16/2/7, SER16/2/8 and SER16/2/9. Further, sample SER16/2/8 is also strongly enriched in all light rare earth elements (LREE) especially Eu, and has one of the higher Eu anomalies (0.77, Table S1). The Eu anomaly, calculated by Eu/Eu^* (where Eu^* is $(Sm_N * Gd_N)^{0.5}$), provides a measure of Eu^{2+} fractionation from Eu^{3+} relative to the neighbouring elements in chondrite normalized rare earth elements (REE). In a sedimentary setting, the calculated values are indicative of source rock types (Kasanzu *et al.* 2008), with a negative anomaly associated with felsic rocks (feldspar bearing rocks), and no anomaly with mafic inputs (Cullers 1994; Gao & Wedepohl 1995; Gallet *et al.* 1998). The negative Eu/Eu* values suggest felsic inputs in all samples, although

samples with the highest values (e.g. SER16/2/8) indicate incorporation of more mafic material. Thus, these samples might have slightly different source rocks, or additions from another source that is affecting the bulk sample geochemical signals. While links between provenance change and quartz signal characteristics are not clear yet, a mechanism could be envisaged where non sensitised quartz grains from smaller, proximal source rocks are added (Pietsch *et al.* 2008; Fitzsimmons 2011). It is beyond the scope of this paper to explore the properties (e.g. components, sensitivity) of the luminescence signal in quartz, and how these are influenced by changes in geochemistry of the sediment or the provenance. However, this section shows the potential for linking geochemical properties with luminescence properties and highlights the need for further investigation.

On the basis of preheat plateau tests, dose recovery tests, the fast ratio and bulk sample geochemistry, quartz OSL signals are considered suitable for dating for most of the samples in Surduk 2A, where calculated D_es are less than 100 Gy, and are not in saturation. Therefore, ages from Surduk 2A are based on quartz signals, apart from samples SER16/2/7 and SER16/2/8, which are excluded from further analyses due to the poor preheat test and recycling ratio performances (SER16/2/7), and non-dominance of the fast component (SER16/2/8). In section Surduk 2B, quartz D_e values exceed 175 Gy for all samples (Table 2). Multiple studies have suggested that quartz OSL ages become less reliable when the D_e is in the 100–200 Gy bracket (e.g. Buylaert *et al.* 2012) due to signal saturation, and the large asymmetric uncer-
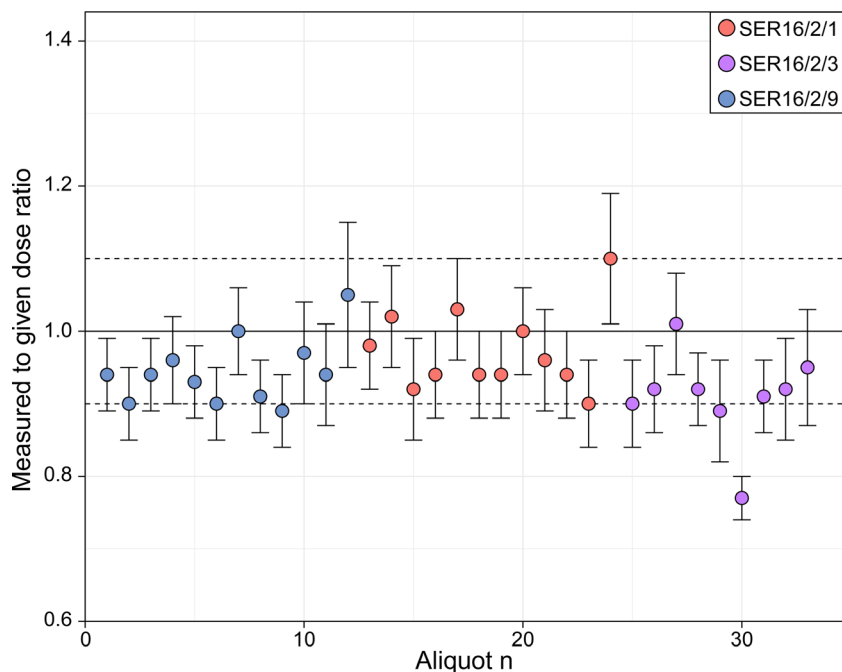
Fig. 4. Quartz dose recovery for samples SER16/2/1, SER16/2/2 and SER16/2/9. Dotted lines mark ±10% from unity.

tainties that result from interpolating onto the asymptote of the dose-response curve (e.g. Fig. 5A). Therefore, for samples with D_es above 100 Gy and SER16/2/7, the D_e was determined using 4–11 μm polymineral fraction and the pIRIR signal.

pIR-IRSL measurements

D_es from polymineral aliquots were calculated using a modified pIRIR SAR protocol (after Thomsen *et al.* 2008; Buylaert *et al.* 2012). In all cases, after a preheat, IR_{50} and $pIRIR_{elev}$ signals were measured for 200 s. The same sequence was followed for the test dose measurement with the addition of a 290 °C 'hot-bleach' (for 200 s) at the end of each cycle. Signals from the first 2 s of stimulation were integrated, with the background taken from the final 100 s of measurements subtracted. An exponential function was used to fit dose-response curves.

Preheat temperature selection

A number of loess luminescence studies from the Carpathian Basin have reported problems with dose recovery when using an elevated temperature pIRIR protocol (Stevens *et al.* 2011; Schatz *et al.* 2012; Murray *et al.* 2014; Újvári *et al.* 2014), especially the 320 °C preheat – 290 °C stimulation temperature combination. Further, research by Roberts (2012) demonstrated the influence of preheat temperature in the pIRIR protocol on the final D_e value, and

therefore the importance of a preheat plateau test for feldspar and polymineral samples. The impact of temperature on D_es was tested through preheat plateau (Fig. 7). Six preheat and elevated pIRIR temperature combinations (three aliquots for each) were analysed, with the pIRIR measurement temperature ~25–30 °C lower than the preheat temperature. For preheats above 280 °C, higher D_es were measured with the $pIRIR_{290}$ protocol (preheat of 320 °C) producing D_es almost twice as large (274±76 Gy) as those in the 225–280 °C temperature range (average 153±5 Gy). These results support observations of Murray *et al.* (2009) and Roberts (2012) who also noted changes in D_es with an increased preheat temperature, which is most likely resulting from sensitivity change occurring between Ln and Tn cycles, which cannot be measured and therefore accounted for (Roberts 2012). The overlapping D_e values for 225–280 °C preheats suggests the preheat plateau is achieved for these temperatures. Therefore, two of the lower temperatures, 220 and 250 °C, were selected for further dose recovery testing.

Residuals

Buylaert *et al.* (2011) and Sohbati *et al.* (2012) indicated that parts of the feldspar signal may be unbleachable, which may affect the ability to recover given doses. Further, if these 'residual' components are large enough they could have an effect on D_e calculation, and therefore age. While many regional loess studies have reported

Table 1. Residual, dose recovery and fading results for selected samples. Fading values and errors reported as means calculated based on three aliquots. * = residual subtracted dose recovery ratio.

Sample	Quartz	Polymineral			
	Dose recovery*	Residual dose (Gy)	Dose recovery*	IR_{50} g-value (%)	$pIRIR_{225}$ g-value (%)
SER16/2/1	0.96±0.06	–	–	–	–
SER16/2/3	0.91±0.06	–	–	–	–
SER16/2/7	–	–	–	13.0±0.9	2.1±1.1
SER16/2/9	0.94±0.06	1.10±0.16	1.08±0.04	–	–
SER16/2/10	–	1.25±0.31	0.87±0.05	16.3±0.9	0.9±1.1
SER16/2/12	–	–	–	11.9±1.0	2.1±1.2
SER16/2/17	–	2.07±0.17	0.87±0.04	10.2±0.9	2.5±1.1
SER16/2/23	–	1.23±0.16	–	5.4±1.2	1.8±1.0
Average	0.94±0.06	1.41±0.20	0.92±0.04	11.37±0.99	1.87±1.11

minimal unbleachable components (Schatz *et al.* 2012; Murray *et al.* 2014; Újvári *et al.* 2014), some have shown quite large residual signals e.g. 15–20 Gy (Austria; Thiel *et al.* 2011) and up to 40 Gy (in some Serbian samples; Stevens *et al.* 2011), demonstrating the importance of testing for this component.
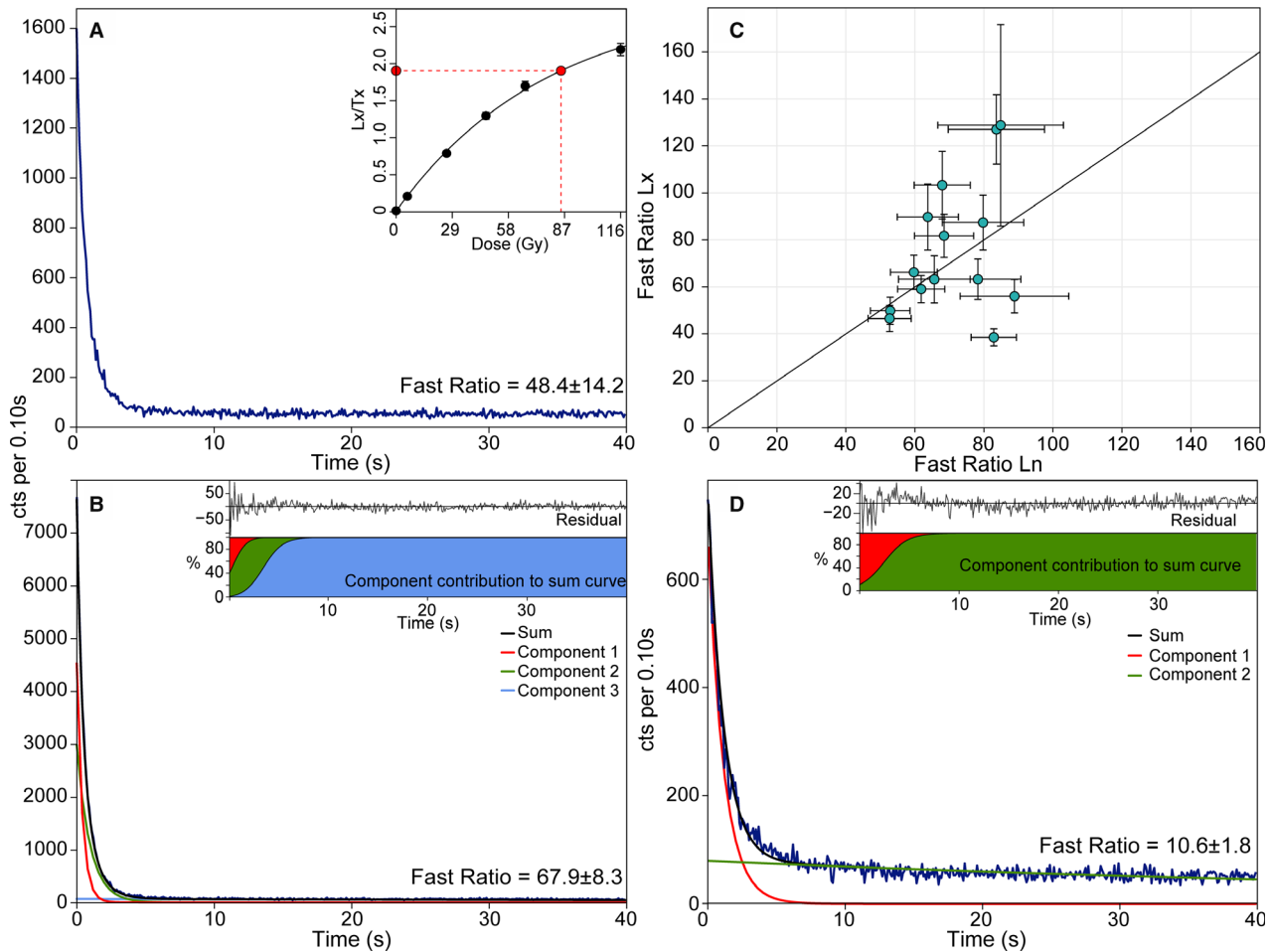

Fig. 5. A. Decay and dose-response curves for quartz (SER16/2/4). B. Decay curve for a typical quartz disc from sample SER16/2/7 with fitted components; insert shows component contributions to the total curve and residuals from the component fitting. C. Fast ratio from the natural signal measurement as a function of fast ratio from the nearest regeneration point for sample SER16/2/7. D. Decay curve for typical quartz disc from sample SER16/2/8 with fitted components; insert shows component contributions to the total curve and residuals from the component fitting. All fast ratios are presented with absolute error values.

To test the size of the residual component in the Surduk 2 samples, six aliquots from four samples, SER16/2/9, SER16/2/10, SER16/2/17, SER16/2/23, were bleached in daylight for 7 days (during May in the UK), and measured using the pIRIR$_{220}$ protocol. Of the 24 aliquots measured, 18 passed the recycling ratio, but none passed a 5% recuperation ratio. As the initial assessment of the signal suggested small natural signals, all recuperation values were converted into absolute values (in Gy) to test for absolute size.

The average residual component measured is 1.41±0.20 Gy (1.10±0.16–2.07±0.17 Gy range; Table 1), equivalent to ~0.4 ka (when calculated using the average polymineral dose rate). These results show that the unbleachable component has a negligible impact on the final ages. It is not possible to compare these values with the previous Surduk 1 study as the residual test was not performed (Fuchs *et al.* 2008). Previously reported Serbian values range between 1 and 40 Gy (Stevens *et al.* 2011; Murray *et al.* 2014; Bösken *et al.* 2017), and along with our results, demonstrate that residual components are sample and site specific, and should be routinely assessed.

Dose recovery

As with quartz, the suitability of the pIRIR protocol was tested using a dose recovery test. First, two pIRIR protocols, pIRIR$_{200}$ (225 °C preheat) and pIRIR$_{225}$ (250 °C), were tested using sample SER16/2/9. Six aliquots were bleached in daylight for 7 days (during May in the UK), irradiated with a laboratory beta-dose approximating their natural one, and measured using the two protocols. Figure 8 shows that the pIRIR$_{225}$ protocol struggled to recover the given dose with an average given to measured ratio of 1.38±0.06. Aliquots measured using the pIRIR$_{200}$ protocol recovered the laboratory dose, giving an average ratio of 1.08±0.04. Subtracting the average residual value from the measured equivalent dose prior to the calculation of the dose recovery takes the ratios down to 1.36±0.06 for pIRIR$_{225}$, while the pIRIR$_{200}$ remains unchanged due to the very small size of residual dose. These results show that the lower preheat temperature better recovers a known dose for this sample.

Following selection of the pIRIR$_{200}$ protocol an additional 12 aliquots per sample (SER16/2/10 and
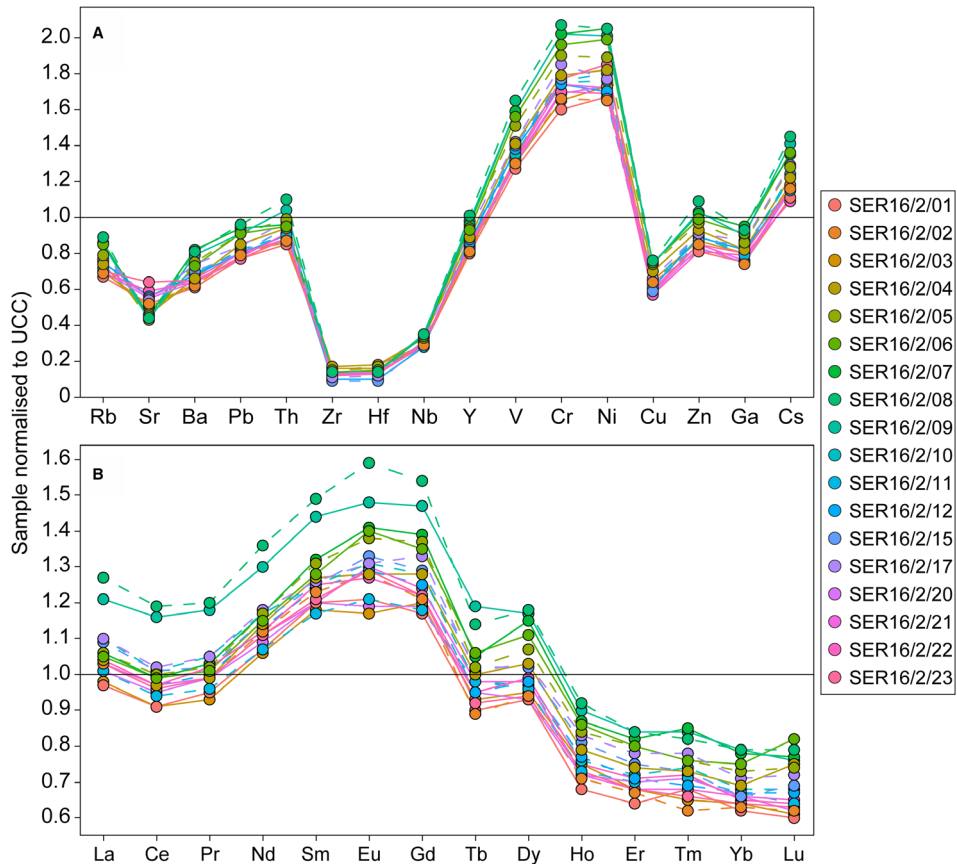

Fig. 6. Bulk sample trace elements UCC-normalized spider diagrams for Surduk 2. A. Large-ion lithophile elements (LILE) and high-field-strength elements (HFSE) elements. B. Light earth elements (LREE) and heavy earth elements (HREE).

Table 2. Samples, depths, radionuclide concentrations, dose rates, D_e values and the final luminescence ages obtained from the 4–11 μm quartz (OSL protocol) and polymineral fractions (pIRIR$_{220}$ protocol). Values are presented to two decimal places, and all calculations were made prior to rounding. Based on the results of the fading correction no fading corrections have been made and therefore the pIRIR$_{200}$ age reflects the uncorrected age. * = overdispersion.

| Sample	Depth (m)	Unit	U (ppm±1σ)	Th (ppm±1σ)	Rb (ppm±1σ)	K (%±1σ)	Quartz					Polymineral			
							Cosmic dose rate (Gy ka⁻¹)	Total dose rate (Gy ka⁻¹)	OD %*	D_e (Gy)	OSL age (ka)	Total dose rate (Gy ka⁻¹)	OD %*	D_e (Gy)	pIRIR$_{220}$ age (ka)
SER16/2/1	1.5	II	1.91±0.19	9.06±0.91	74.64±7.46	1.88±0.19	0.18±0.02	3.19±0.22	9	64.52±1.88	20.23±1.49	–	–	–	–
SER16/2/2	1.8	II	1.86±0.19	9.29±0.93	76.73±7.67	2.08±0.21	0.17±0.02	3.36±0.23	1.5	67.69±0.93	20.13±1.40	–	–	–	–
SER16/2/3	2.1	II	2.54±0.25	9.20±0.92	78.64±7.86	2.27±0.23	0.16±0.02	3.72±0.26	3.3	70.13±1.25	18.85±1.33	–	–	–	–
SER16/2/4	2.4	II	2.21±0.22	10.02±1.0	83.43±8.34	2.47±0.25	0.16±0.02	3.87±0.27	5.6	86.43±1.90	22.35±1.61	–	–	–	–
SER16/2/5	2.7	II	2.10±0.21	10.02±1.0	87.78±8.78	2.26±0.23	0.15±0.02	3.64±0.25	4.4	82.05±2.23	22.52±1.66	–	–	–	–
SER16/2/6	3	II	2.06±0.21	10.19±1.02	94.94±9.49	2.27±0.23	0.15±0.02	3.65±0.25	7.5	85.27±2.07	23.37±1.70	–	–	–	–
SER16/2/7	3.3	II	2.04±0.20	10.26±1.03	95.80±9.58	2.38±0.24	0.14±0.01	–	–	–	–	4.40±0.28	2.6	99.24±1.39	22.57±1.46
SER16/2/8	3.6	II	2.14±0.21	11.82±1.18	100.03±10.0	2.43±0.24	0.14±0.01	3.95±0.27	5.4	84.58±1.96	21.43±1.57	–	–	–	–
SER16/2/9	3.9	II	2.08±0.21	11.08±1.11	95.52±9.55	2.37±0.24	0.13±0.01	3.81±0.26	7.4	92.73±2.36	24.35±1.79	–	–	–	–
SER16/2/10	4.4	IV	1.86±0.19	9.79±0.98	81.13±8.11	1.92±0.19	0.14±0.01	3.23±0.22	0	175.66±3.63	54.45±3.92	3.84±0.24	9	174.34±5.87	45.46±3.26
SER16/2/23	4.8	IV	1.89±0.19	9.47±0.95	78.49±7.85	1.83±0.18	0.13±0.01	3.12±0.22	17	120.61±7.50	38.60±3.58	3.73±0.24	3.6	176.16±2.80	47.29±3.09
SER16/2/12	5.2	IV	1.81±0.18	9.67±0.97	83.85±8.39	1.93±0.19	0.13±0.01	3.20±0.22	4.6	169.94±3.89	53.09±3.87	3.80±0.24	4	179.77±3.29	47.33±3.12
SER16/2/22	5.5	IV	1.98±0.20	9.73±0.97	76.73±7.67	1.80±0.18	0.12±0.01	–	–	–	–	3.76±0.24	0	187.56±2.46	49.94±3.24
SER16/2/21	5.8	IV	1.98±0.20	9.42±0.94	80.88±8.09	1.82±0.18	0.12±0.01	–	–	–	–	3.48±0.23	1.3	186.19±2.45	49.77±3.22
SER16/2/20	6.1	IV	1.92±0.19	9.41±0.94	78.42±7.84	1.80±0.18	0.12±0.01	3.09±0.21	0	200.13±3.94	64.83±4.67	3.69±0.23	0	191.85±2.56	51.99±3.37
SER16/2/15	6.4	IV	1.89±0.19	10.11±1.01	85.83±8.58	1.90±0.19	0.11±0.01	–	–	–	–	3.85±0.25	2	196.20±2.64	50.95±3.32
SER16/2/17	7.2	V	1.99±0.20	10.48±1.05	88.84±8.88	1.85±0.19	0.11±0.01	3.23±0.23	4	193.33±5.03	59.78±4.46	3.89±0.25	0	199.32±2.75	51.30±3.36
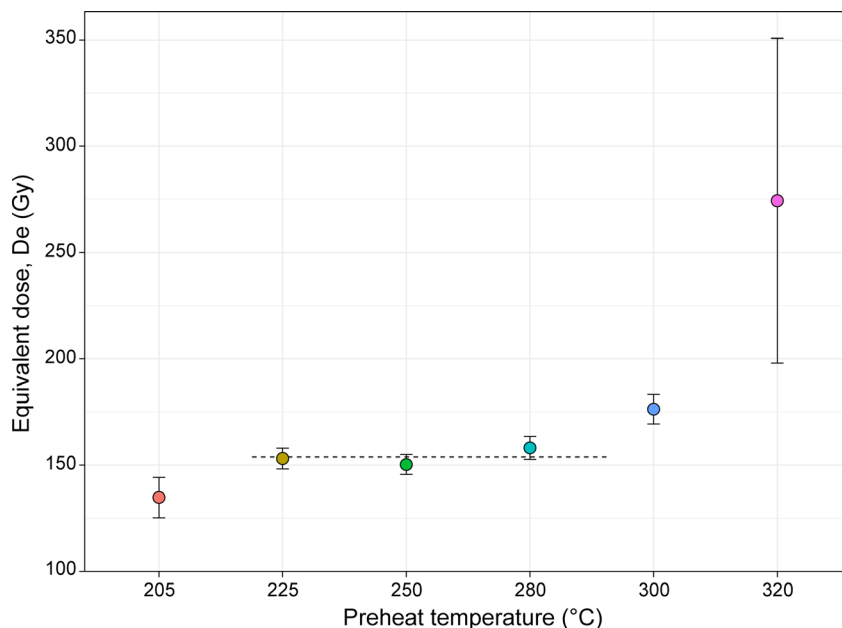
Fig. 7. D_e dependency on preheat temperature for sample SER16/2/9. The average D_e and standard deviation of three aliquots at each temperature are shown. Note the preheat plateau (dashed line) marked for the temperature range 225–280 °C.

SER16/2/17) were analysed following the same preparation and measurement protocol. The average measured to given dose ratio for these samples was 0.92 ± 0.04 ($n = 18$), suggesting a satisfactory pIRIR protocol for D_e measurement.

Laboratory fading

Laboratory fading rates ($g_{2\ days}$) were tested for the $pIRIR_{200}$ signal, using the same protocol used for D_e measurements. Following Auclair *et al.* (2003) three aliquots per sample were irradiated with a fixed dose (~90 Gy), a test dose (~40 Gy) and measured following a series of pauses (0, 1, 10, 100 and 1000 h). The mean fading rates for the IR_{50} and $pIRIR_{200}$ signals are $11.37\pm0.99\%$/decade and $1.87\pm1.11\%$/decade ($n = 15$, five samples), respectively. The range of the fading rates for the IR_{50} signal varies between 0.43 ± 0.94 and $21.53\pm0.74\%$/decade, whereas the $pIRIR_{200}$ results range from 0.27 ± 0.92 to $3.46\pm1.23\%$/decade (Fig. 9, Table 1). These results demonstrate that IR_{50} signals undergo high rates of fading at Surduk 2. In contrast, fading rates for the $pIRIR_{220}$ are sufficiently low that they do not require a fading correction, following the arguments of Buylaert *et al.* (2012) and Thiel *et al.* (2011).

D_e and age calculation

All measured aliquots ($n = 345$) were screened using signal recuperation (<5%), a recycling ratio (Murray & Wintle 2000), and additionally for quartz, an OSL IR depletion ratio (Duller 2003). In total, 24 signals were rejected due to a failed recycling ratio, and six signals failed recuperation. All but five quartz signals passed the IR depletion ratio. Overdispersion (Table 2) was found to be below 10% (except for the quartz sample SER16/2/23) and therefore all equivalent doses were calculated using the central age model (CAM; Galbraith *et al.* 1999). CAM D_es were divided by the environmental dose rate to derive the age. As discussed, D_es were calculated from quartz for Surduk 2A samples, with the exception of SER16/2/7 and SER16/2/8. For all other samples, polymineral pIRIR signals were used.

Age-depth-model and MARs

All final luminescence ages were re-calculated using Bayesian and inverse modelling (Zeeden *et al.* 2018), which separates systematic and random errors of luminescence ages. This model creates probability density functions for both types of error but models only the random component of the uncertainty, making this approach better suited for the analysis of luminescence ages than other Bayesian models such as OxCal (Bronk Ramsey 1995). Due to the lack of overlap and to uncertainty regarding the sediment thickness, two separate models were created: one for Surduk 2A and the second for Surduk 2B. These age-depth models provide a basis for calculating sediment accumulation rates, as well as a better visual representation of the age distribution throughout the profile.

Loess–palaeosol sequences can preserve information about dust fluxes, yet to date no sites from Europe have
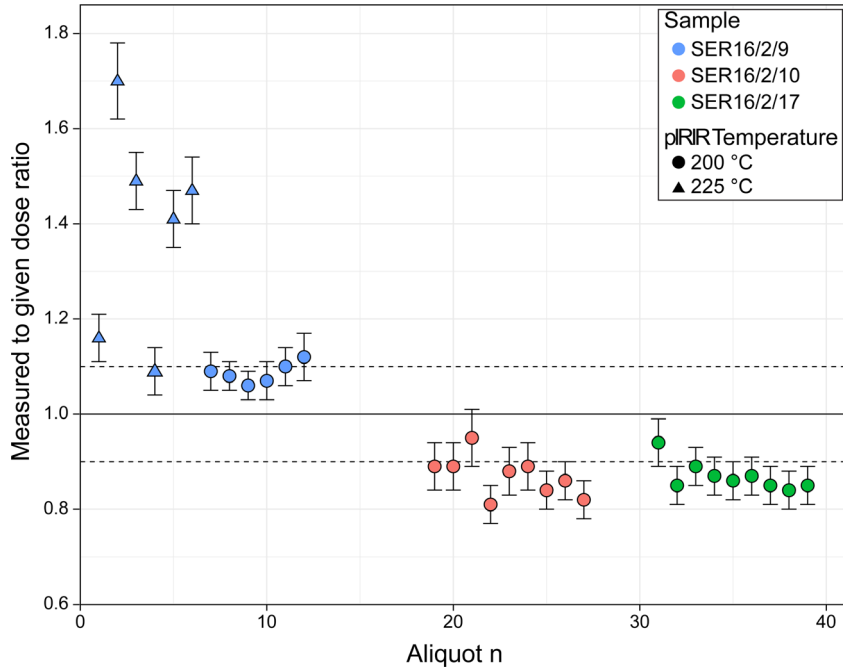
Fig. 8. Polymineral dose recovery for samples SER16/2/9, SER16/2/10 and SER16/2/17. Note dose recovery tests for the pIRIR$_{220}$ and pIRIR$_{225}$ protocols were carried out using sample SER16/2/9. Dotted lines mark ±10% from unity. All samples had a residual dose subtracted prior to the calculation.

been included in the global palaeodust cycle modelling efforts (Albani *et al.* 2015), mostly resulting from the lack of high-resolution chronologies. To aid those efforts, a number of loess studies (Újvári *et al.* 2015; Stevens *et al.* 2016; Perić *et al.* 2019) have converted age-depth models into MARs. Here, modelled luminescence ages
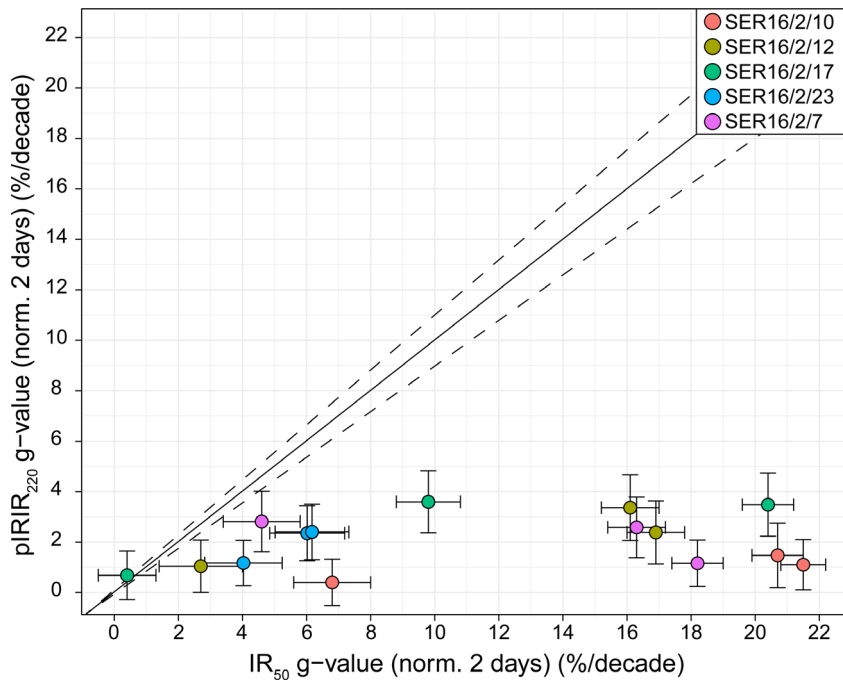

Fig. 9. Calculated fading rates for the IR$_{50}$ and pIRIR$_{200}$ luminescence signals for all aliquots.

were used to calculate MARs (Kohfeld & Harrison 2003) using the following equation

$$MAR\,(g\,m^{-2}a^{-1}) = SR \times f_{eol} \times \rho_{dry} \qquad (1)$$

where SR is the sedimentation rate (m a^{-1}), f_{eol} is the fraction of the sediment that is aeolian in origin, and ρ_{dry} is the bulk density of dry sediment (g m^{-3}). As the sediment is interpreted as loess and therefore aeolian in origin, $f_{eol} = 1$. A bulk density value of 1.5 g cm^{-3} was used in all calculations based on the reported estimates of loess bulk density in Hungary and Serbia (Újvári *et al.* 2010; Perić *et al.* 2019). Finally, in desert research it has been shown that using only mean ages to construct sedimentation rates for sand dune accumulation may provide an inaccurate picture of aeolian and climatic history (Leighton *et al.* 2014), therefore for the first time in loess research two MARs are calculated based on mean and minimal sedimentation rates. Mean sedimentation rates are calculated as $SR_{mean} = x_1 - x_2/y_1 - y_2$, where x_{1-2} are two depths and y_{1-2} corresponding ages in the profile. The $SR_{min} = x_1 - x_2/((y_1 + \sigma_1) - (y_2 - \sigma_2))$ also includes age errors for each relative age.

To ensure a meaningful and fair comparison of MARs between loess studies, only sites with a high-resolution, absolute chronology were selected. Further, sites where the luminescence chronology used an IR_{50} signal that had not been tested for fading were also excluded. Therefore, three sites, Crvenka (Stevens *et al.* 2011), Dunaszekcső (Újvári *et al.* 2017) and Titel (Perić *et al.* 2019), were selected for MAR assessment.

Palaeoenvironmental results and discussion

A new chronology and sedimentation rates for the Surduk 2 loess–palaeosol sequence

Unmodelled quartz and polymineral pIRIR$_{200}$ luminescence ages for Surduk 2 are presented in Table 2. The preferred (see Quartz quartz signal assessment and provenance discussion) unmodelled and modelled ages are presented in Fig. 10 and Table S2. Sixteen ages span from the top of the transitional palaeosol (Unit III) to 1.5 m below the modern-day surface. All but one of the ages come from loess Unit II, with the youngest age 19.03±1.03 ka. The bottom age, for the transitional zone between palaeosol and loess, places its burial at 52.55±2.71 ka.

The ages for both parts of the profile form two stratigraphically consistent depositional groups. The first (Surduk 2A) covers 1.5 m within the top ~4 m and represents the period between 19.03±1.03 and 24.62±1.31 ka. The second group (Surduk 2B) consists of eight samples, spread over 2.8 m, with ages between 44.99±2.20 and 52.55±2.71 ka. These two groups are separated by a sampling gap that is estimated to be

between 1 and 1.5 m. The comparison of ages above and below shows relatively rapid accumulation rates and suggests that within that packet of sediment a change occurred. Without further high-resolution chronological investigation at this stage, it is not possible to definitively determine whether this gap represents a period of sediment accumulation lows, driven by environmental or climatic factors, or if this is an erosion boundary between different periods of dust accumulation. However, it is most likely that an erosional boundary is present above L1LL2, supporting a previously argued notion that loess sequences are neither continuous nor homogenous, and are likely to preserve disturbances in deposition (Stevens *et al.* 2008, 2018).

Comparison with other sites and implications

The oldest age obtained from Surduk 2B comes from the transitional palaeosol-loess zone near the bottom of the profile and dates sediment burial to 52.55±2.71 ka. The calcification and compaction of the palaeosol below precluded collection of samples and determination of the beginning of deposition for this part of the profile/sequence. The comparison of the basal parts between Surduk 1 and 2 shows a large age discrepancy (Fig. 10). Based on stratigraphical position, the bottom palaeosol at Surduk 2B may correspond either with the 'Basal soil complex' or the 'Middle soil complex' at Surduk 1, and therefore be interpreted as either S1 or L1SS2 palaeosol.

The loess deposition on top of the 'Basal soil complex' at Surduk 1 was dated to 82.6±9.0 ka (Fig. 10). Due to the blanket nature of loess deposition, it is highly unlikely that there is a 'real' ~30-ka discrepancy between Surduk 2 and Surduk 1 deposits, especially given that they are located so closely together. The luminescence investigation at Surduk 1 did not test the IR_{50} signal for fading and ages were not corrected (Fuchs *et al.* 2008). Fading tests at Surduk 2 show that the polymineral IR_{50} signal is athermally unstable (Fig. 9). Similar fading behaviour can be expected from Surduk 1, and it is likely that Surduk 1's chronology underestimates the true ages. Therefore, the age of 82.6±9.0 ka for the 'Basal soil complex' at Surduk 1 is likely to be too young. However, without fading rate data for those samples, combined with the old age of the samples (and therefore the difficulties in correcting the non-linear part of the dose-response curve), it is not reasonable to speculate upon the degree of under-estimation of each age at Surduk 1 in Fuchs *et al.* (2008). Nonetheless taking the fading rates broadly into consideration and the depths of the units at both profiles, it is likely that the Unit VI palaeosol at Surduk 2B corresponds with the 'Middle soil complex' at Surduk 1, dated to 36.3±4.1 ka (Fuchs *et al.* 2008).

Nevertheless, if the correlation based on stratigraphy was correct, it would suggest favourable pedogenic conditions at Surduk 2B persisting until 52.55±2.71
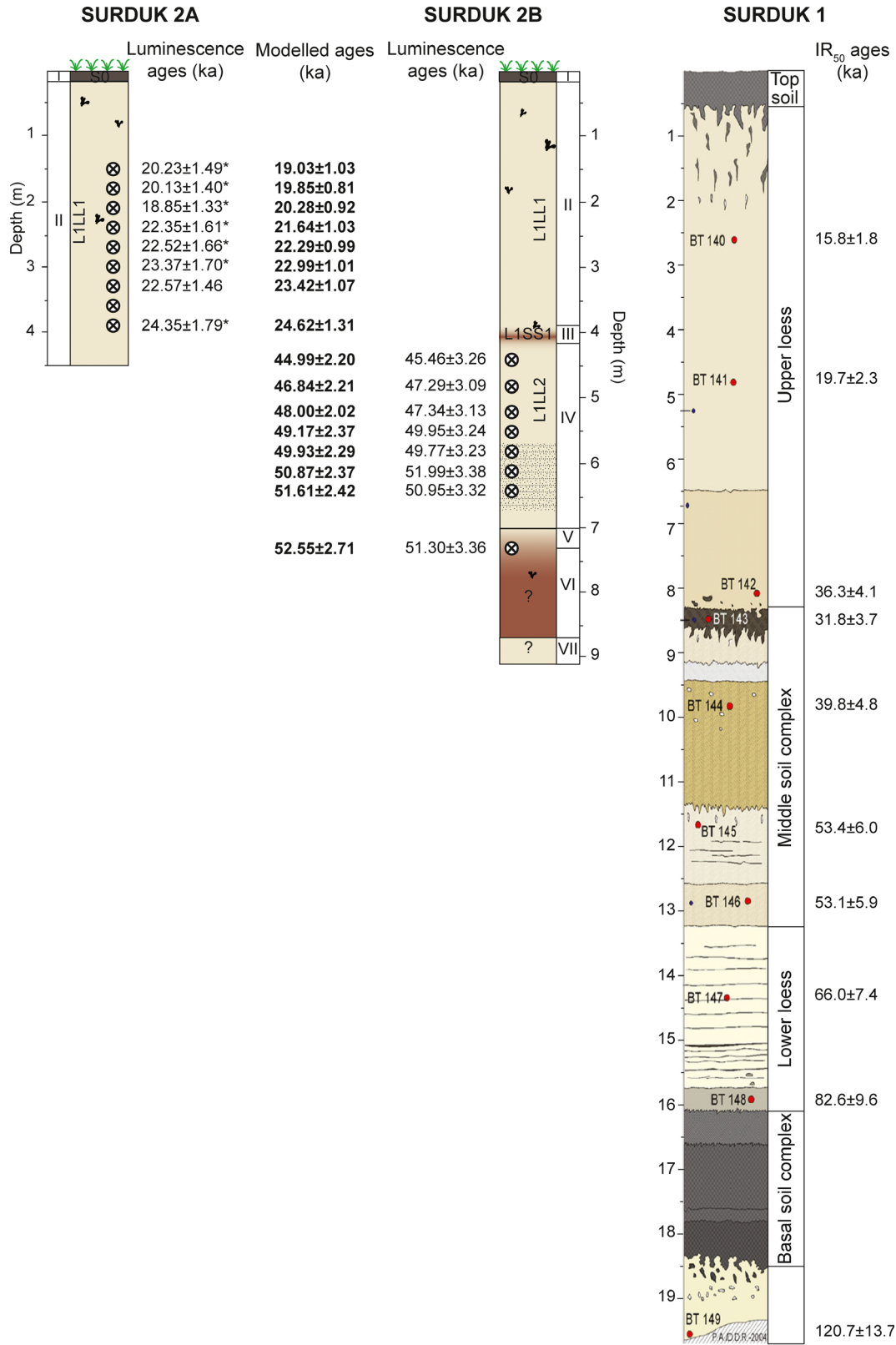
Fig. 10. Schematic stratigraphical diagram for Surduk 1 (Fuchs *et al.* 2008; Antoine *et al.* 2009) and Surduk 2. For the Surduk 2 quartz OSL (marked by *), polymineral pIRIR$_{220}$ and Bayesian modelled ages (bold) are presented.
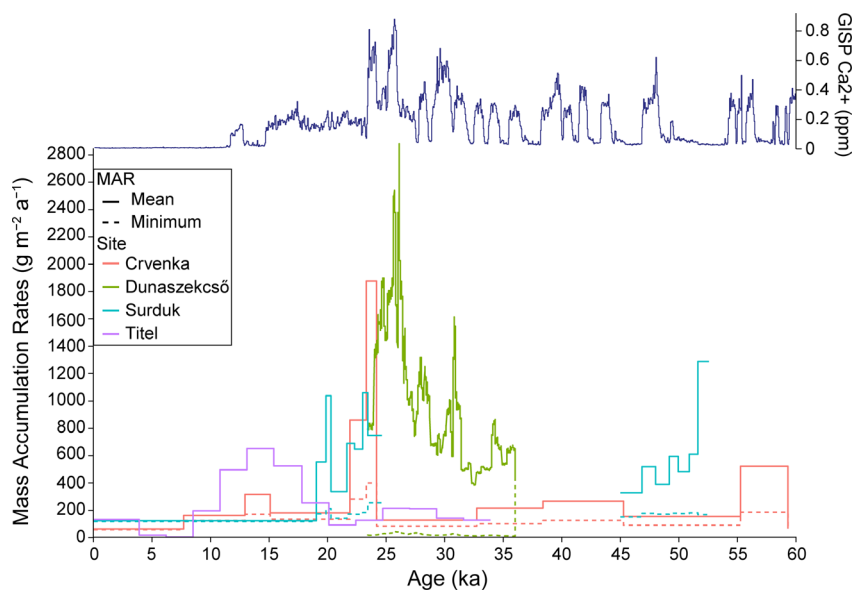
Fig. 11. Mass accumulation rates (MARs) as a function of age for the loess–palaeosol profile at Surduk 2, plotted against results from Titel (Perić *et al.* 2019), Dunaszekcső (Újvári *et al.* 2017), Crvenka (Stevens *et al.* 2011), and the GISP Ca^{2+} record (Rasmussen *et al.* 2014). The geographical location of these sites in relation to Surduk 2 is shown in Fig. 1.

ka, and no loess deposits corresponding to the initial climate deterioration seen across the region and associated with MIS 3 (Bokhorst *et al.* 2011; Panagiotopoulos *et al.* 2014; Wegwerth *et al.* 2016). This could be a result of repeated erosional events at Surduk 2, possible due to the geomorphic position of the site. Alternatively, a number of loess profiles in central Europe e.g. Stalać (Bösken *et al.* 2017), Süttő (Novothny *et al.* 2009), and Stari Slankamen (Schmidt *et al.* 2010), indicate persistent pedogenesis until the MIS 3 stage, which may have also occurred at Surduk. However, without further geochronological investigation at Surduk 1, it is not possible to determine if the stratigraphic discrepancy between Surduk 1 and 2 palaeosols represents: multiple erosional events at Surduk 2; differences in pedogenic conditions; or a chronological discrepancy.

Following the transitional unit, primary loess deposition began at Surduk 2B after 52.55±2.71 ka and lasted at least until 44.99±2.20 ka (Fig. 10). At the beginning of this period, the mass accumulation rates were the highest in the profile, 1288 $g\,m^{-2}\,a^{-1}$ (mean; minimum = 163 $g\,m^{-2}\,a^{-1}$), after which they decreased in a step-like manner all the way up through Unit IV (Fig. 11). However, there are two brief periods of increased accumulation between 49.93±2.29 and 49.17±2.37 ka (mean 591 $g\,m^{-2}\,a^{-1}$ and min. 174 $g\,m^{-2}\,a^{-1}$) and 48.00±2.02 and 46.84±2.21 ka (mean 514 $g\,m^{-2}\,a^{-1}$ and min. 173 $g\,m^{-2}\,a^{-1}$). This indicates temporary environmental deterioration or increased supply of material during the early MIS 3. While a decrease in MAR values is also seen in Crvenka over this period (Stevens *et al.* 2011), the lack of a temporary increase could be

attributed to the lower chronological resolution of the study or the site's position. We propose that the increase in accumulation was locally driven and probably related to the site's proximity to the Danube and sediment source. Further, it is important to note that while mean rates show a relatively large change in the MAR values, e.g. from 607 to 479 $g\,m^{-2}\,a^{-1}$, the difference in minimum rates is very small (176 and 171 $g\,m^{-2}\,a^{-1}$). Seeing that these rates are almost three times lower and do not really show corresponding trends, this highlights that care must be taken when interpreting MARs, especially when only mean rates are presented.

A hiatus in luminescence ages is observed between 44.99±2.20 and 24.62±1.31 ka. At present, it is not possible to determine the source of this discrepancy (sedimentary hiatus or sedimentation slowdown) or the exact position of the gap. Consequently, the record of the early MIS 3 sedimentation is missing from Surduk 2. The MIS 3 period was considered a climatically milder and more stable component of the previous interglacial (Wegwerth *et al.* 2015), but containing pronounced oscillations (Hoffecker 2009; Fischer *et al.* 2017). At other loess profiles, e.g. Belotinac (Obreht *et al.* 2014), Crvenka (Stevens *et al.* 2011; Zech *et al.* 2013), Dunaszekcső (Újvári *et al.* 2014), Stari Slankamen (Schmidt *et al.* 2010), Stalać (Bösken *et al.* 2017) and Tokaj (Schatz *et al.* 2012), it is associated with palaeosol development. A hint of a weak pedogenic horizon was observed in the field above the sample SER16/2/10 but this part of the section was not accessible at the time.

In the later parts of MIS 3, the climate in the region is suggested to have been progressively deteriorating, with

colder temperatures, increased precipitation, and changes in vegetation cover (Kageyama *et al.* 2006; Sümegi *et al.* 2013, 2019; Zech *et al.* 2013). This can be seen represented at other sites such as Dunaszekcső (Újvári *et al.* 2017) or Titel (Perić *et al.* 2019) by an increase in MAR values, which is expected as the ice sheets grow to their maximum extent. Taking this regional picture into consideration, we suggest that Surduk 2 contains a sedimentological hiatus, and if a palaeosol was present, it has likely been eroded. It is not possible to determine how much sediment has been removed as only the remaining features are datable. However, a further higher resolution chronological investigation should be able to identify when exactly the gap occurs.

The top part of Unit II preserves ~5.5 ka of dust accumulation and represents the prelude to, and the main part of the Last Glacial Maximum (LGM). While not particularly thick in comparison to other loess sections recording this period of accumulation, it still indicates progressive and relatively rapid sediment accumulation from 24.62 ± 1.31 ka (mean 744 g m^{-2} a^{-1}; Fig. 11). This period of deposition also corresponds to a potential shift in provenance. Bulk sample geochemical analyses (Fig. 6) suggest sediment at that time had slightly more mafic and/or less felsic source rock inputs. The analysis did not imply complete change in provenance but rather small contributions from other sources. This temporary shift combined with a short-distance transport could indicate sediment delivered to the site from relatively proximal rocks, likely linked to landscape instability during the build-up to the LGM.

Following this period at 23.42 ± 1.07 ka (Fig. 11), MARs rose to the second highest values for Surduk 2 (mean 1058 g m^{-2} a^{-1}), indicating increased environmental instability. High MARs did not persist for long and began to drop after 22.99 ± 1.01 ka and continued to fall until 20.28 ± 0.92 ka (mean 333 g m^{-2} a^{-1}). This was followed by a temporary rise to the second highest rate at Surduk 2A (mean 1036 g m^{-2} a^{-1} and min. 207 g m^{-2} a^{-1}) that lasted until 19.85 ± 0.81 ka. These results indicate that even during the LGM, which is thought to be the period of highest sediment accumulation, the deposition was not constant.

The values at Surduk 2 are as much as five times greater than those shown for this period at the nearby Titel Plateau (Perić *et al.* 2019), which are exceeded even by the conservative minimum values of 207 g m^{-2} a^{-1}. While the Surduk 1 profile does not fully capture a chronology for this period, it still suggests increased wind speeds or delivery of coarser material to the system as a higher proportion of sands and reduction of clay is noted (Antoine *et al.* 2009), further supporting a lack of vegetation and cold/windy conditions.

The uppermost sample at Surduk 2, located 1.5 m below the modern land surface, indicates loess deposition at 19.03 ± 1.03 ka (Fig. 10). It is expected that during deglaciation and a transition to the Holocene, sediment availability declined and depositional rates decreased as vegetation became more established. The transition to the Holocene palaeosol is not strongly marked or visible. A lack of thick well-developed Holocene soil, as well as a thicker deglaciation loess unit, is also seen at Surduk 1. Moreover, considering human activities on the modern land surface at both localities, it is likely that Holocene soil (S0) has been removed as part of agricultural processes.

Comparison with Greenland and implications for MAR interpretations

A number of studies have attempted to link central European loess deposits with Greenland dust records based on geochemistry (Újvári *et al.* 2015), MARs (Újvári *et al.* 2017), particle size (e.g. Rousseau *et al.* 2002; Antoine *et al.* 2009) and models (e.g. Sima *et al.* 2009) to show loess contributions to the global dust record. Figure 11 shows MARs from four sites around the southern part of the Carpathian Basin plotted against dust records from Greenland (Rasmussen *et al.* 2014). Firstly, and most notably, it can be observed that peaks and troughs in accumulation do not always overlap. While some broad similarities are seen, records often conflict with each other, e.g. Surduk 2 MARs show increased accumulation followed by a decrease at around 23 ka; however, at the same time at Crvenka rates fall dramatically and stabilize for several thousands of years. It must be pointed out that with higher dating resolution less of the sedimentary sequence is averaged, hence records from sites such as Dunaszekcső show much more detail and variability by comparison. Even if broad trends can be seen there appears to be Carpathian Basin wide heterogeneity, with no obvious trends in accumulation seen over relatively short distances. This suggests that loess does not develop as a blanket feature at the same time across the landscape, as sediment is not transported to the sites uniformly. The comparison between sites in the Carpathian Basin thus suggests that accumulation at each site is likely driven by short-distance transport and local factors, such as sediment availability on flood-plains.

When further compared with the dust record from Greenland (Fig. 11) the picture is quite complex. The MAR patterns seen in the Carpathian Basin do not always mirror trends in Greenland. For example, during the drop in accumulation between 51.61 ± 2.42 and 50.87 ± 2.37 ka at Surduk 2 (shift from 1288 to 607 g m^{-2} a^{-1}) values in Greenland remained relatively constant. At the same time while Surduk 2 notes high rates of accumulation the dust flux in Greenland is low. However, the drop–rise pattern between 50–47 ka at Surduk 2 approximates the pattern seen in Greenland. In both cases, increases in MARs at Surduk 2 precede changes in Greenland, although dust flux ceased at the same time.

The same pattern is also observed for peaks at 20.28±0.92 ka at Surduk 2A and smaller peak at ~28 ka at Dunaszekcső (Újvári *et al.* 2017). It could be therefore argued that for some instances the record from the Carpathian Basin is preceding the changes that are eventually picked up in Greenland.

Lastly, it is important to note how much variability is seen between the mean and minimum MAR rates. Calculating minimum MAR values takes into account the uncertainty of ages and enables a fuller exploration of the geomorphological signal. For the most part, the same trends are still seen between minimum and mean values but the discrepancy between the two values can reach almost two orders of magnitude (e.g. Dunaszekcső). This approach is not taken to discredit the mean values, but to highlight that the true MAR values are somewhere in between the minimum and maximum (which is often impossible to calculate). Therefore, while the trends can be explored when using mean values alone, interpretation of values where only mean values are presented should be taken with caution, especially when comparing with other dust records, such as Greenland. Finally, this point is particularly pertinent to the debate surrounding the contributions of European loess deposits to the dust recorded in Greenland (Sima *et al.* 2009; Albani *et al.* 2015; Újvári *et al.* 2015, 2017). It is unlikely that a sole site was contributing greatly, but the lack of overlapping trends between sites and the discrepancy between minimum and mean rates suggest that European loess contributions are periodic, and secondary. However, more sites with higher resolution chronologies are needed to unpack this complex dust record, and its contribution to global dust archives.

Conclusions

This study presents a new high-resolution chronology for the loess–palaeosol sequence at Surduk 2, based on 13 quartz OSL and 10 polymineral pIRIR$_{220}$ ages, that provides a basis for a broad review of the palaeoenvironmental record preserved at this site. The modelled luminescence ages based on both protocols bracket the primary loess deposition between 52.55±2.71 and 19.03±1.03 ka. The results, however, suggest that this record is not continuous and contains a hiatus that occurred after 44.99±2.20 ka and prior to 24.62±1.31 ka. The bulk sample elemental analysis identified a potential abrupt but small provenance shift that occurred between 24.62±1.31 and 23.42±1.07 ka. Further, the high-resolution chronology provides a basis for calculation of MARs for Surduk 2 and comparison with other sites from the Carpathian Basin, Crvenka (Stevens *et al.* 2011), Dunaszekcső (Újvári *et al.* 2017), Titel (Perić *et al.* 2019) and Greenland (Rasmussen *et al.* 2014). The analysis demonstrates that sites experienced increased periods of accumulation at different times, showing that sites' depositional histories are not uniform, despite their

relatively close locations. Therefore, preserved loess sequences likely depend on a site's geomorphological position and palaeotopography, which control the appearance and intensity of erosional and pedogenic processes (Vandenberghe *et al.* 2014; Marković *et al.* 2018). While European loess contributions to Greenland are still debated, these results suggest that they do not play a major role. Finally, we suggest that additional chronological analysis is needed to identify the exact position of the hiatus and to determine how long this site was stabilized for prior to 53 ka and whether it experienced pedogenically favourable conditions continuously since the last interglacial.

Author contributions. – SBM assisted KF with sample collection. All laboratory analysis, including sediment dating, writing, and figure and table preparation was conducted by KF. JAD assisted with luminescence experiments planning, and discussion of results. JAD, DSGT, ILM and SBM provided comments prior to paper submission.

References

Aitken, M. J. 1985: *Thermoluminescence Dating.* 351 pp. Academic Press, London.

Aitken, M. J. 1998: *An Introduction to Optical Dating. The Dating of Quaternary Sediments by the Use of Photon-Stimulated Luminescence.* 267 pp. Oxford University Press, Oxford.

Albani, S., Mahowald, N. M., Winckler, G., Anderson, R. F., Bradtmiller, L. I., Delmonte, B., François, R., Goman, M., Heavens, N. G., Hesse, P. P., Hovan, S. A., Kang, S. G., Kohfeld, K. E., Lu, H., Maggi, V., Mason, J. A., Mayewski, P. A., McGee, D., Miao, X., Otto-Bliesner, B. L., Perry, A. T., Pourmand, A., Roberts, H. M., Rosenbloom, N., Stevens, T. & Sun, J. 2015: Twelve thousand years of dust: The Holocene global dust cycle constrained by natural archives. *Climate of the Past 11,* 869–903.

Antoine, P., Rousseau, D.-D., Fuchs, M., Hatté, C., Gauthier, C., Marković, S. B., Jovanović, M., Gaudenyi, T., Moine, O. & Rossignol, J. 2009: High-resolution record of the last climatic cycle in the southern Carpathian Basin (Surduk, Vojvodina, Serbia). *Quaternary International 198,* 19–36.

Auclair, M., Lamothe, M. & Huot, S. 2003: Measurement of anomalous fading for feldspar IRSL using SAR. *Radiation Measurements 37,* 487–492.

Bailey, R. M., Smith, B. W. & Rhodes, E. J. 1997: Partial bleaching and the decay form characteristics of quartz OSL. *Radiation Measurements 27,* 123–136.

Bokhorst, M. P., Vandenberghe, J., Sümegi, P., Łanczont, M., Gerasimenko, N. P., Matviishina, Z. N., Marković, S. B. & Frechen, M. 2011: Atmospheric circulation patterns in central and eastern Europe during the Weichselian Pleniglacial inferred from loess grain-size records. *Quaternary International 234,* 62–74.

Bösken, J., Klasen, N., Zeeden, C., Obreht, I., Marković, S. B., Hambach, U. & Lehmkuhl, F. 2017: New luminescence-based geochronology framing the last two glacial cycles at the southern limit of European Pleistocene loess in Stalać (Serbia). *Geochronometria 44,* 150–161.

Bøtter-Jensen, L., Bulur, E., Duller, G. A. T. & Murray, A. S. 2000: Advances in luminescence instrument systems. *Radiation Measurements 32,* 523–528.

Bracciali, L., Marroni, M., Pandolfi, L. & Rocchi, S. 2007: Geochemistry and petrography of Western Tethys Cretaceous sedimentary covers (Corsica and Northern Apennines): from source areas to configuration of margins. *Special Paper of the Geological Society of America 420*, 73–93.

Brennan, B. J., Lyons, R. G. & Phillips, S. W. 1991: Attenuation of alpha particle track dose for spherical grains. *International Journal of Radiation Applications and Instrumentation, Part 18*, 249–253.

Bronk Ramsey, C. 1995: Radiocarbon calibration and analysis of stratigraphy: the OxCal program. *Radiocarbon 37*, 425–430.

Bronk Ramsey, C. 2008: Radiocarbon dating: revolutions in understanding. *Archaeometry 50*, 249–275.

Buylaert, J.-P., Jain, M., Murray, A. S., Thomsen, K. J., Thiel, C. & Sohbati, R. 2012: A robust feldspar luminescence dating method for Middle and Late Pleistocene sediments. *Boreas 41*, 435–451.

Buylaert, J.-P., Thiel, C., Murray, A. S., Vandenberghe, D. A. G., Yi, S. & Lu, H. 2011: IRSL and post-IR IRSL residual doses recorded in modern dust samples from the Chinese Loess Plateau. *Geochronometria 38*, 432–440.

Cullers, R. L. 1994: The controls on the major and trace element variation of shales, siltstones, and sandstones of Pennsylvanian-Permian age from uplifted continental blocks in Colorado to platform sediment in Kansas, USA. *Geochimica et Cosmochimica Acta 58*, 4955–4972.

Duller, G. A. T. 2003: Distinguishing quartz and feldspar in single grain luminescence measurements. *Radiation Measurements 37*, 161–165.

Durcan, J. A. & Duller, G. A. T. 2011: The fast ratio: a rapid measure for testing the dominance of the fast component in the initial OSL signal from quartz. *Radiation Measurements 46*, 1065–1072.

Durcan, J. A., King, G. E. & Duller, G. A. T. 2015: DRAC: Dose Rate and Age Calculator for trapped charge dating. *Quaternary Geochronology 28*, 54–61.

Fischer, P., Hambach, U., Klasen, N., Schulte, P., Zeeden, C., Steininger, F., Lehmkuhl, F., Gerlach, R. & Radtke, U. 2017: Landscape instability at the end of MIS 3 in western Central Europe: evidence from a multi proxy study on a loess-palaeosol-sequence from the eastern Lower Rhine Embayment, Germany. *Quaternary International 502*, 119–136.

Fitzsimmons, K. E. 2011: An assessment of the luminescence sensitivity of Australian quartz with respect to sediment history. *Geochronometria 38*, 199–208.

Fitzsimmons, K. E., Marković, S. B. & Hambach, U. 2012: Pleistocene environmental dynamics recorded in the loess of the middle and lower Danube basin. *Quaternary Science Reviews 41*, 104–118.

Frechen, M., Horváth, E. & Gábris, G. 1997: Geochronology of Middle and Upper Pleistocene Loess Sections in Hungary. *Quaternary Research 312*, 291–312.

Frechen, M., Oches, E. A. & Kohfeld, K. E. 2003: Loess in Europe - Mass accumulation rates during the Last Glacial Period. *Quaternary Science Reviews 22*, 1835–1857.

Fuchs, M., Kreutzer, S., Rousseau, D.-D., Antoine, P., Hatté, C., Lagroix, F., Moine, O., Gauthier, C., Svoboda, J. & Lisá, L. 2013: The loess sequence of Dolní Věstonice, Czech Republic: a new OSL-based chronology of the Last Climatic Cycle. *Boreas 42*, 664–677.

Fuchs, M., Rousseau, D.-D., Antoine, P., Hatté, C., Gauthier, C., Marković, S. B. & Zöeller, L. 2008: Chronology of the Last Climatic Cycle (Upper Pleistocene) of the Surduk loess sequence, Vojvodina, Serbia. *Boreas 37*, 66–73.

Galbraith, R. F., Roberts, R. G., Laslett, G. M., Yoshida, H. & Olley, J. M. 1999: Optical Dating of Single and Multiple Grains of Quartz From Jinmium Rock Shelter, Northern Australia: Part I, Experimental Design and Statistical Models. *Archaeometry 41*, 365–395.

Gallet, S., Jahn, B., Lano, B. V. V., Dia, A. & Rossello, E. 1998: Loess geochemistry and its implications for particle origin and composition of the upper continental crust. *Earth and Planetary Science Letters 156*, 157–172.

Galović, L., Frechen, M., Halamić, J., Durn, G. & Romić, M. 2009: Loess chronostratigraphy in Eastern Croatia – a luminescence dating approach. *Quaternary International 198*, 85–97.

Gao, S. & Wedepohl, K. H. 1995: The negative Eu anomaly in Archean sedimentary rocks: implications for decomposition, age and impor-

tance of their granitic sources. *Earth and Planetary Science Letters 133*, 81–94.

Gasparon, M., Innocenti, F., Manetti, P., Peccerillo, A. & Tsegaye, A. 1993: Genesis of the Pliocene to Recent bimodal mafic-felsic volcanism in the Debre Zeyt area, central Ethiopia: volcanological and geochemical constraints. *Journal of African Earth Sciences 17*, 145–165.

Götte, T. & Ramseyer, K. 2012: Trace element characteristics, luminescence properties and real structure of quartz. *In* Götze, J. & Möckel, R. (eds.): *Quartz: Deposits, Mineralogy and Analytics*, 265–285. Springer, Berlin.

Gray, H. J., Jain, M., Sawakuchi, A. O., Mahan, S. A. & Tucker, G. E. 2019: Luminescence as a sediment tracer and provenance tool. *Reviews of Geophysics 57*, 987–1017.

Guérin, G., Mercier, N. & Adamiec, G. 2011: Dose-rate conversion factors: update. *Ancient TL 29*, 5–8.

Hatté, C., Gauthier, C., Rousseau, D.-D., Antoine, P., Fuchs, M., Lagroix, F., Marković, S. B., Moine, O. & Sima, A. 2013: Excursions to C 4 vegetation recorded in the upper Pleistocene loess of SURDUK (Northern Serbia): an organic isotope geochemistry study. *Climate of the Past 9*, 1001–1014.

Hoffecker, J. F. 2009: The spread of modern humans in Europe. *Proceedings of the National Academy of Sciences of the United States of America 106*, 16040–16045.

Huntley, D. J. & Lamothe, M. 2001: Ubiquity of anomalous fading in K-feldspars and the measurement and correction for it in optical dating. *Canadian Journal of Earth Sciences 38*, 1093–1106.

Kageyama, M., Laine, A., Abe-Ouchi, A., Braconnot, P., Cortijo, E., Crucifix, M., de Vernal, A., Guiot, J., Hewitt, C. D., Kitoh, A., Kucera, M., Marti, O. & Ohgaito, R. 2006: Last Glacial Maximum temperatures over the North Atlantic, Europe and western Siberia: a comparison between PMIP models, MARGO sea – surface temperatures and pollen-based reconstructions. *Quaternary Science Reviews 25*, 2082–2102.

Kars, R. H., Wallinga, J. & Cohen, K. M. 2008: A new approach towards anomalous fading correction for feldspar IRSL dating - tests on samples in field saturation. *Radiation Measurements 43*, 786–790.

Kasanzu, C., Maboko, M. A. H. & Manya, S. 2008: Geochemistry of fine-grained clastic sedimentary rocks of the Neoproterozoic Ikorongo Group, NE Tanzania: implications for provenance and source rock weathering. *Precambrian Research 164*, 201–213.

King, G. E., Durcan, J. A. & Burow, C. 2019: *calc_FastRatio: Calculate the Fast Ratio for CW-OSL curves. Function version 0.1.1. Luminescence: Comprehensive Luminescence Dating Data Analysis R package version 0.9.3.*

Kohfeld, K. E. & Harrison, S. P. 2003: Glacial-interglacial changes in dust deposition on the Chinese Loess Plateau. *Quaternary Science Reviews 22*, 1859–1878.

Kreutzer, S. 2019: fit_CWCurve: Nonlinear Least Squares Fit for CW-OSL curves. *In* Kreutzer, S., Burow, C., Dietze, M., Fuchs, M. C., Schmidt, C., Fischer, M. & Friedrich, J. (eds.): *Luminescence: Comprehensive Luminescence Dating Data Analysis R Package Version 0.9.3.*

Kreutzer, S., Schmidt, C., Dewitt, R. & Fuchs, M. 2014: The a-value of polymineral fine grain samples measured with the post-IR IRSL protocol. *Radiation Measurements 69*, 18–29.

Leighton, C. L., Thomas, D. S. G. & Bailey, R. M. 2014: Reproducibility and utility of dune luminescence chronologies. *Earth-Science Reviews 129*, 24–39.

Li, B. & Li, S.-H. 2008: Investigations of the dose-dependent anomalous fading rate of feldspar from sediments. *Journal of Physics D: Applied Physics 41*, 225502, https://doi.org/10.1088/0022-3727/41/22/225502.

Mahowald, N. M., Muhs, D. R., Levis, S., Rasch, P. J., Yoshioka, M., Zender, C. S. & Luo, C. 2006: Change in atmospheric mineral aerosols in response to climate: last glacial period, preindustrial, modern, and doubled carbon dioxide climates. *Journal of Geophysical Research: Atmospheres 111*, D10202, https://doi.org/10.1029/2005JD006653.

Marković, S. B., Hambach, U., Catto, N., Jovanović, M., Buggle, B., Machalett, B., Zöller, L., Glaser, B. & Frechen, M. 2009: Middle and late Pleistocene loess sequences at Batajnica, Vojvodina, Serbia. *Quaternary International 198*, 255–266.

Marković, S. B., Hambach, U., Stevens, T., Jovanović, M., O'Hara-Dhand, K., Basarin, B., Lu, H., Smalley, I. J., Buggle, B., Zech, M., Svirčev, Z., Sümegi, P., Milojković, N. & Zöller, L. 2012: Loess in the Vojvodina region (Northern Serbia): an essential link between European and Asian Pleistocene environments. *Geologie en Mijnbouw/Netherlands Journal of Geosciences 91*, 173–188.

Marković, S. B., Hambach, U., Stevens, T., Kukla, G. J., Heller, F., McCoy, W. D., Oches, E. A., Buggle, B. & Zöller, L. 2011: The last million years recorded at the Stari Slankamen (North Serbia) loess-paleosol sequence: revised chronostratigraphy and long-term environmental trends. *Quaternary Science Reviews 30*, 1142–1154.

Marković, S. B., Stevens, T., Kukla, G. J., Hambach, U., Fitzsimmons, K. E., Gibbard, P., Buggle, B., Zech, M., Guo, Z., Hao, Q., Wu, H., O'Hara-Dhand, K., Smalley, I. J., Újvári, G., Sümegi, P., Timar-Gabor, A., Veres, D., Sirocko, F., Vasiljević, D. A., Jary, Z., Svensson, A. M., Jović, V., Lehmkuhl, F., Kovács, J. & Svirčev, Z. 2015: Danube loess stratigraphy - Towards a pan-European loess stratigraphic model. *Earth-Science Reviews 148*, 228–258.

Marković, S. B., Stevens, T., Mason, J. A., Vandenberghe, J., Yang, S., Veres, D., Újvári, G., Timar-Gabor, A., Zeeden, C., Guo, Z., Hao, Q., Obreht, I., Hambach, U., Wu, H., Gavrilov, M. B., Rolf, C., Tomić, N. & Lehmkuhl, F. 2018: Loess correlations – Between myth and reality. *Palaeogeography, Palaeoclimatology, Palaeoecology 509*, 4–23.

Mejdahl, V. 1979: Thermoluminescence dating: beta-dose attenuation in quartz grains. *Archaeometry 21*, 61–72.

Moine, O., Antoine, P., Hatté, C., Landais, A., Mathieu, J., Prud'homme, C. & Rousseau, D.-D. 2017: The impact of Last Glacial climate variability in west-European loess revealed by radiocarbon dating of fossil earthworm granules. *Proceedings of the National Academy of Sciences of the United States of America 114*, 6209–6214.

Morthekai, P., Jain, M., Murray, A. S., Thomsen, K. J. & Botter-Jensen, L. 2008: Fading characteristics of martian analogue materials and the applicability of a correction procedure. *Radiation Measurements 43*, 672–678.

Muhs, D. R. 2013: The geologic records of dust in the Quaternary. *Aeolian Research 9*, 3–48.

Murray, A. S. & Wintle, A. G. 1999: Isothermal decay of optically stimulated luminescence in quartz. *Radiation Measurements 30*, 119–125.

Murray, A. S. & Wintle, A. G. 2000: Luminescence dating of quartz using an improved single-aliquot regenerative-dose protocol. *Radiation Measurements 32*, 57–73.

Murray, A. S., Buylaert, J.-P., Thomsen, K. J. & Jain, M. 2009: The effect of preheating on the IRSL signal from feldspar. *Radiation Measurements 44*, 554–559.

Murray, A. S., Schmidt, E. D., Stevens, T., Buylaert, J.-P., Marković, S. B., Tsukamoto, S. & Frechen, M. 2014: Dating Middle Pleistocene loess from Stari Slankamen (Vojvodina, Serbia) - limitations imposed by the saturation behaviour of an elevated temperature IRSL signal. *Catena 117*, 34–42.

Novothny, Á., Frechen, M., Horváth, E., Bradák, B., Oches, E. A., McCoy, W. D. & Stevens, T. 2009: Luminescence and amino acid racemization chronology of the loess–paleosol sequence at Süttő, Hungary. *Quaternary International 198*, 62–76.

Novothny, Á., Horváth, E. & Frechen, M. 2002: The loess profile at Albertirsa, Hungary – improvements in loess stratigraphy by luminescence dating. *Quaternary International 95–96*, 155–163.

Obreht, I., Buggle, B., Catto, N., Marković, S. B., Bösel, S., Vandenberghe, D. A. G., Hambach, U., Svirčev, Z., Lehmkuhl, F., Basarin, B., Gavrilov, M. B. & Jović, G. 2014: The Late Pleistocene Belotinac section (southern Serbia) at the southern limit of the European loess belt: environmental and climate reconstruction using grain size and stable C and N isotopes. *Quaternary International 334–335*, 10–19.

Panagiotopoulos, K., Böhm, A., Leng, M. J., Wagner, B. & Schäbitz, F. 2014: Climate variability over the last 92 ka in SW Balkans from analysis of sediments from Lake Prespa. *Climate of the Past 10*, 643–660.

Perić, Z., Lagerbäck Adolphi, E., Stevens, T., Újvári, G., Zeeden, C., Buylaert, J.-P., Marković, S. B., Hambach, U., Fischer, P., Schmidt, C., Schulte, P., Huayu, L., Shuangwen, Y., Lehmkuhl, F., Obreht, I.,

Veres, D., Thiel, C., Frechen, M., Jain, M., Vött, A., Zöller, L. & Gavrilov, M. B. 2019: Quartz OSL dating of late quaternary Chinese and Serbian loess: a cross Eurasian comparison of dust mass accumulation rates. *Quaternary International 502*, 30–44.

Pietsch, T. J., Olley, J. M. & Nanson, G. C. 2008: Fluvial transport as a natural luminescence sensitiser of quartz. *Quaternary Geochronology 3*, 365–376.

Pigati, J. S., McGeehin, J. P., Muhs, D. R. & Bettis, E. A. 2013: Radiocarbon dating late Quaternary loess deposits using small terrestrial gastropod shells. *Quaternary Science Reviews 76*, 114–128.

Prescott, J. R. & Hutton, J. T. 1994: Cosmic ray contributions to dose rates for luminescence and ESR dating: large depths and long-term time variations. *Radiation Measurements 23*, 497–500.

Preusser, F., Degering, D., Fuchs, M., Hilgers, A., Kadereit, A., Klasen, N., Krbetschek, M., Richter, D. & Spencer, J. Q. G. 2008: Luminescence dating: basics, methods and applications. *Quaternary Science Journal 57*, 95–149.

Rasmussen, S. O., Bigler, M., Blockley, S. P. E., Blunier, T., Buchardt, S. L., Clausen, H. B., Cvijanovic, I., Dahl-Jensen, D., Johnsen, S. J., Fischer, H., Gkinis, V., Guillevic, M., Hoek, W. Z., Lowe, J. J., Pedro, J. B., Popp, T., Seierstad, I. K., Steffensen, J. P., Svensson, A. M., Vallelonga, P., Vinther, B. M., Walker, M. J. C., Wheatley, J. J. & Winstrup, M. 2014: A stratigraphic framework for abrupt climatic changes during the Last Glacial period based on three synchronized Greenland ice-core records: refining and extending the INTIMATE event stratigraphy. *Quaternary Science Reviews 106*, 14–28.

Roberts, H. M. 2012: Testing Post-IR IRSL protocols for minimising fading in feldspars, using Alaskan loess with independent chronological control. *Radiation Measurements 47*, 716–724.

Rodrigues, A. L., Dias, M. I., Valera, A. C., Rocha, F., Prudêncio, M. I. & Marques, R. 2019: Geochemistry, luminescence and innovative dose rate determination of a Chalcolithic calcite-rich negative feature. *Journal of Archaeological Science: Reports 26*, 101887, https://doi.org/10.1016/j.jasrep.2019.101887.

Rousseau, D.-D., Antoine, P., Hatté, C., Lang, A., Zöller, L., Fontugne, M., Othman, D. Ben., Luck, J. M., Moine, O., Labonne, M., Bentaleb, I. & Jolly, D. 2002: Abrupt millennial climatic changes from Nussloch (Germany) Upper Weichselian eolian records during the Last Glaciation. *Quaternary Science Reviews 21*, 1577–1582.

Schatz, A.-K., Buylaert, J.-P., Murray, A. S., Stevens, T. & Scholten, T. 2012: Establishing a luminescence chronology for a palaeosol-loess profile at Tokaj (Hungary): a comparison of quartz OSL and polymineral IRSL signals. *Quaternary Geochronology 10*, 68–74.

Schmidt, E. D., Machalett, B., Marković, S. B., Tsukamoto, S. & Frechen, M. 2010: Luminescence chronology of the upper part of the Stari Slankamen loess sequence (Vojvodina, Serbia). *Quaternary Geochronology 5*, 137–142.

Sima, A., Rousseau, D.-D., Kageyama, M., Ramstein, G., Schulz, M., Balkanski, Y., Antoine, P., Dulac, F. & Hatté, C. 2009: Imprint of North-Atlantic abrupt climate changes on western European loess deposits as viewed in a dust emission model. *Quaternary Science Reviews 28*, 2851–2866.

Smith, B. W. & Rhodes, E. J. 1994: Charge movements in quartz and their relevance to optical dating. *Radiation Measurements 23*, 329–333.

Sohbati, R., Murray, A. S., Buylaert, J.-P., Ortuño, M., Cunha, P. P. & Masana, E. 2012: Luminescence dating of Pleistocene alluvial sediments affected by the Alhama de Murcia fault (eastern Betics, Spain) - a comparison between OSL, IRSL and post-IR IRSL ages. *Boreas 41*, 250–262.

Stevens, T., Adamiec, G., Bird, A. F. & Lu, H. 2013: An abrupt shift in dust source on the Chinese Loess Plateau revealed through high sampling resolution OSL dating. *Quaternary Science Reviews 82*, 121–132.

Stevens, T., Buylaert, J.-P., Lu, H., Thiel, C., Murray, A. S., Frechen, M., Yi, S. & Zeng, L. 2016: Mass accumulation rate and monsoon records from Xifeng, Chinese Loess Plateau, based on a luminescence age model. *Journal of Quaternary Science 31*, 391–405.

Stevens, T., Buylaert, J.-P., Thiel, C., Újvári, G., Yi, S., Murray, A. S., Frechen, M. & Lu, H. 2018: Ice-volume-forced erosion of the Chinese Loess Plateau global Quaternary stratotype site. *Nature Communications 9*, 983, https://doi.org/10.1038/s41467-018-03329-2.

Stevens, T., Lu, H., Thomas, D. S. G. & Armitage, S. J. 2008: Optical dating of abrupt shifts in the late Pleistocene East Asian monsoon. *Geology 36*, 415–418.

Stevens, T., Marković, S. B., Zech, M., Hambach, U. & Sümegi, P. 2011: Dust deposition and climate in the Carpathian Basin over an independently dated last glacial–interglacial cycle. *Quaternary Science Reviews 30*, 662–681.

Sümegi, P., Magyari, E. K., Dániel, P., Molnár, M. & Törocsik, T. 2013: Responses of terrestrial ecosystems to Dansgaard-Oeshger cycles and Heinrich-events: a 28,000-year record of environmental changes from SE Hungary. *Quaternary International 293*, 34–50.

Sümegi, P., Molnár, D., Gulyás, S., Náfrádi, K., Sümegi, B. P., Törőcsik, T., Persaits, G., Molnár, M., Vandenberghe, J. & Zhou, L. 2019: High-resolution proxy record of the environmental response to climatic variations during transition MIS3/MIS2 and MIS2 in Central Europe: the loess-paleosol sequence of Katymár brickyard (Hungary). *Quaternary International 504*, 40–55.

Thiel, C., Buylaert, J.-P., Murray, A. S., Terhorst, B., Hofer, I., Tsukamoto, S. & Frechen, M. 2011: Luminescence dating of the Stratzing loess profile (Austria) – Testing the potential of an elevated temperature post-IR IRSL protocol. *Quaternary International 234*, 23–31.

Thiel, C., Horváth, E. & Frechen, M. 2014: Revisiting the loess/palaeosol sequence in Paks, Hungary: a post-IR IRSL based chronology for the 'Young Loess Series'. *Quaternary International 319*, 88–98.

Thomsen, K. J., Murray, A. S. & Jain, M. 2011: Stability of IRSL signals from sedimentary K-feldspar samples. *Geochronometria 38*, 1–13.

Thomsen, K. J., Murray, A. S., Jain, M. & Bøtter-Jensen, L. 2008: Laboratory fading rates of various luminescence signals from feldspar-rich sediment extracts. *Radiation Measurements 43*, 1474–1486.

Timar-Gabor, A., Constantin, D., Buylaert, J.-P., Jain, M., Murray, A. S. & Wintle, A. G. 2015: Fundamental investigations of natural and laboratory generated SAR dose response curves for quartz OSL in the high dose range. *Radiation Measurements 81*, 150–156.

Újvári, G., Kovács, J., Varga, G., Raucsik, B. & Marković, S. B. 2010: Dust flux estimates for the Last Glacial Period in East Central Europe based on terrestrial records of loess deposits: a review. *Quaternary Science Reviews 29*, 3157–3166.

Újvári, G., Molnár, M., Novothny, Á., Páll-Gergely, B., Kovács, J. & Várhegyi, A. 2014: AMS 14C and OSL/IRSL dating of the Dunaszekcső loess sequence (Hungary): chronology for 20 to 150ka and implications for establishing reliable age-depth models for the last 40ka. *Quaternary Science Reviews 106*, 140–154.

Újvári, G., Stevens, T., Molnár, M., Demény, A., Lambert, F., Varga, G., Jull, A. J. T., Páll-Gergely, B., Buylaert, J.-P. & Kovács, J. 2017: Coupled European and Greenland last glacial dust activity driven by North Atlantic climate. *Proceedings of the National Academy of Sciences of the United States of America 114*, E10632–E10638.

Újvári, G., Stevens, T., Svensson, A. M., Klötzli, U. S., Manning, C. J., Németh, T., Kovács, J., Sweeney, M. R., Gocke, M., Wiesenberg, G. L. B., Marković, S. B. & Zech, M. 2015: Two possible source regions for central Greenland last glacial dust. *Geophysical Research Letters 42*, 10399–10408.

Vandenberghe, J., Marković, S. B., Jovanovič, M. & Hambach, U. 2014: Site-specific variability of loess and palaeosols (Ruma, Vojvodina, northern Serbia). *Quaternary International 334–335*, 86–93.

Wegwerth, A., Ganopolski, A., Ménot, G., Kaiser, J., Dellwig, O., Bard, E., Lamy, F. & Arz, H. W. 2015: Black Sea temperature response to glacial millennial-scale climate variability. *Geophysical Research Letters 42*, 8147–8154.

Wegwerth, A., Kaiser, J., Dellwig, O., Shumilovskikh, L. S., Nowaczyk, N. R. & Arz, H. W. 2016: Northern hemisphere climate control on the environmental dynamics in the glacial Black Sea 'Lake'. *Quaternary Science Reviews 135*, 41–53.

Wintle, A. G. 1973: Anomalous fading of thermo-luminescence in mineral samples. *Nature 245*, 143–144.

Wintle, A. G. & Murray, A. S. 2006: A review of quartz optically stimulated luminescence characteristics and their relevance in single-aliquot regeneration dating protocols. *Radiation Measurements 41*, 369–391.

Zech, R., Zech, M., Marković, S. B., Hambach, U. & Huang, Y. 2013: Humid glacials, arid interglacials? Critical thoughts on pedogenesis and paleoclimate based on multi-proxy analyses of the loess-paleosol sequence Crvenka, Northern Serbia. *Palaeogeography, Palaeoclimatology, Palaeoecology 387*, 165–175.

Zeeden, C., Dietze, M. & Kreutzer, S. 2018: Discriminating luminescence age uncertainty composition for a robust Bayesian modelling. *Quaternary Geochronology 43*, 30–39.

Supporting Information

Additional Supporting Information may be found in the online version of this article at http://www.boreas.dk.

Table S1. Raw bulk sample geochemical composition for loess–palaeosol samples from Surduk 2 profile.

Table S2. The unmodelled and modelled ages for loess-palaeosol samples from Surduk 2 profile.